Biophysical Journal
Article

Biophysical Society

SxIP binding disrupts the constitutive homodimer interface of EB1 and stabilizes EB1 monomer

Shine Ayyappan,[1] Pooja S. Dharan,[1] Arya Krishnan,[2] Renjith R. Marira,[2] Mahil Lambert,[1] Tapas K. Manna,[2] and Vinesh Vijayan[1,*]
[1]School of Chemistry and [2]School of Biology, Indian Institute of Science Education and Research, Thiruvananthapuram, Kerala, India

ABSTRACT SxIP is a microtubule tip localizing signal found in many +TIP proteins that bind to the hydrophobic cavity of the C-terminal domain of end binding protein 1 (EB1) and then positively regulate the microtubule plus-end tracking of EBs. However, the exact mechanism of microtubule activation of EBs in the presence of SxIP signaling motif is not known. Here, we studied the effect of SxIP peptide on the native conformation of EB1 in solution. Using various NMR experiments, we found that SxIP peptide promoted the dissociation of natively formed EB1 dimer. We also discovered that I224A mutation of EB1 resulted in an unfolded C-terminal domain, which upon binding with the SxIP motif folded to its native structure. Molecular dynamics simulations also confirmed the relative structural stability of EB1 monomer in the SxIP bound state. Residual dipolar couplings and heteronuclear NOE analysis suggested that the binding of SxIP peptide at the C-terminal domain of EB1 decreased the dynamics and conformational flexibility of the N-terminal domain involved in EB1-microtubule interaction. The SxIP-induced disruption of the dimeric interactions in EB1, coupled with the reduction in conformational flexibility of the N-terminal domain of EB1, might facilitate the microtubule association of EB1.

SIGNIFICANCE Our study aims to understand the SxIP-mediated dynamic stability of EB1 protein in solution. Using NMR as a primary method, we determined that SxIP binding destabilizes EB1 dimer. Further, SxIP binding promoted the folding of the unstructured C-terminal domain of EB1 (I224A) mutant. Additionally, we also discovered that SxIP modulates the backbone dynamic of the N-terminal domain of EB1 by reducing the EB1n-EB1n and EB1n-EB1c transient interactions. The previously unknown outcome of the binding of SxIP with EB1 is thus elucidated, which could be significant in elucidating the mechanism of EB1 activation.

INTRODUCTION

Microtubules (MTs) are highly dynamic tubule-like polymers of α- and β-tubulin heterodimers found in the cytoplasm of eukaryotic cells (1,2). MTs act as a major constituent of the cytoskeleton and regulate vital cellular processes such as intracellular transport, chromosome segregation, cellular organization, etc. (3,4). These polymers consist of a relatively stable minus end and an extremely dynamic plus end, which switch between the phases of growth and shortening, called dynamic instability (4–6). The plus-end tracking proteins (+TIPs) localize at the plus end of MTs and regulate the MT plus-end dynamics, thus controlling the various microtubule-mediated cellular processes (7–10).

EB1 (end-binding protein-1) is a conserved member of the +TIPs. The protein exists as a homodimer and consists of a globular N-terminus (EB1n, 1–130), an unstructured linker region (131–189), and a coiled-coil C-terminal domain (EB1c, 190–268) (11,12). EB1n specifically recognizes the GTP-bound tubulin subunits found at the plus end of MTs (13–16). EB1c is subdivided into a coiled-coil region, called the EB homology domain (EBH, 222–254), and a disordered tail containing a specific EEY/F sequence motif (17). The EBH domain consists of a four-helix bundle, composed of mostly hydrophobic residues (17). EBH domain promotes the EB1 dimerization that is observed in the native structure. EB1 autonomously tracks to the dynamic end of MTs and additionally recruits other +TIPs to the plus end (18,19). Therefore, EB1 is considered as a master regulator of dynamic events at the plus end of MTs (20).

The majority of the +TIPs that do not have the inherent ability to localize with microtubules have conserved peptide

Submitted November 16, 2020, and accepted for publication March 1, 2021.
*Correspondence: vinesh@iisertvm.ac.in
Editor: Scott Showalter.
https://doi.org/10.1016/j.bpj.2021.03.004

motifs responsible for their EB1 recognition and their subsequent recruitment to the MTs. SxIP (x for any amino acid) and GKNDG motifs are the two well-known conserved peptide-signaling sequences found in most of the +TIPs (21–23). Recently, a new signaling motif, LxxPTPh (x for any amino acid; h represents the hydrophobic residue) is also observed in various +TIPs (24). The +TIPS bind to EB1c domain and subsequently target the respective proteins toward the MTs (25–27). EB1 protein also showed a significant increase in their MT localization with the addition of these peptide signals (26,28,29). Hence, characterizing the EB1 interaction with the signaling motifs of the +TIPS is vital for understanding the mechanism of the recruitment of the protein to the plus end of the microtubule.

The crystal structure of the complex formed by EB1c and GKNDG signaling motif of P150N protein showed that the GKNDG signals specifically recognized the extreme C-terminal EEY/F amino acid sequence of EB1 (26). A proposed model for the activation of EB1 by GKNDG signaling motif described the apo EB1 in an autoinhibitory state, with the extreme C-terminal end of EB1 masking the microtubule-binding site of EB1n. The binding of the GKNDG motif to the extreme C-terminal end of EB1 destabilizes the closed conformation of EB1, which consequently increases the microtubule localization of EB1.

The SxIP-sequence containing proteins constitutes a large group of structurally heterogeneous +TIPs (APC, CLASP1/2, DDA3, etc.) that are recruited by EB1 to MTs. Associations of several such EB-binding +TIPs have been characterized (30–32). The reported crystal structure of EB1c-bound MACF2 protein has an SxIP motif bound to the hydrophobic C-terminal part of EB1c but distinct from the binding site of the GKNDG signaling motif (33). Also, similar to the GKNDG +TIPs, the SxIP proteins activated the microtubule localization of EB1 (29). But the exact mechanism for the increased microtubule association of EB1 by SxIP signaling motifs remained unknown. Moreover, most structural studies on EB1 have been carried out on the individual domains of EB1, and the effect of SxIP on the full-length protein has not been characterized. The crystal structures of apo EB1n and EB1c domains, as well as NMR studies on the individual domains, were known (11,17,34), but no NMR or x-ray studies on the full-length protein have been carried out so far.

Here, we studied the effect of SxIP peptide binding on the full-length EB1 using NMR spectroscopy. We hypothesized that because EB1n binds to MT, the conformational change in EBH domain brought about by the binding of SxIP motifs should translate and modulate the dynamics of EB1n, which in turn regulate the binding of EB1 to MT. The dynamics could either disrupt the EB1n-EB1n interaction or EB1n-EB1c interactions that masks the binding site for the MTs. Our studies clearly showed that the binding of SxIP signals induced the dissociation of EB1 homodimer and stabilized the monomer form. The stability of the monomeric structure was further supported by NMR analysis of an EB1 monomer-specific mutant wherein the SxIP binding drove the folding of the EB1c domain. SxIP binding also decreased the conformational flexibility of the N-terminal domain of EB1, and that possibly favors EB1 localization of MTs.

MATERIALS AND METHODS

A detailed description of the materials and methods for this work used can be found in the Supporting materials and methods.

RESULTS AND DISCUSSION

Transient interactions in EB1

The presence of both EB1n-EB1c and EB1n-EB1n interactions was previously reported (34,35). The autoinhibitory interaction between the EB1c domain and EB1n domain was already known (26). The binding surface of EB1c on EB1n, composed of residues H18, K62, H69, E70, K100, D125, A128, and R130, was previously determined using NMR spectroscopy (34). The NMR titration experiments suggested a weak binding between EB1c and EB1n, as only a decrease in intensity of residues in EB1n was observed. Previous studies with cross-linking experiments and subsequent mass spectrometric analysis showed that K113 and K122 were part of EB1n-EB1n interactions (35). However, a complete set of residues required for defining the binding surface of EB1n-EB1n interactions were yet to be determined. To determine the N-terminal dimer interface, we performed a concentration-dependent NMR titration experiment of only the EB1n domain. The ^{1}H-^{15}N HSQC spectra of EB1n at two different concentrations (0.075 and 1.25 mM) were compared (Fig. 1, *A* and *B*). The association of protein was confirmed from the nearly uniform increase in the linewidth of almost all NMR peaks of EB1n at the higher concentration (Fig. 1 *C*). A set of residues showed a more significant increase in linewidth than average (Fig. 1 *C*). These residues were mapped on the crystal structure of EB1n (Fig. 1 *E*). The most affected residues because of EB1n-EB1n interactions were S16, N25, L32, T33, I35, F47, G54, F63, Q79, F82, K100, F105, F107, K112, K113, and F115. It is also to be noted that in the full-length EB1 protein, because of the orientational constraints of the C-terminal dimer, some of the EB1n-EB1n interactions that we observe might be absent. The increase in the linewidth of NMR peaks with increasing concentration of EB1n suggested transient EB1n-EB1n association (Fig. 1 *D*). Therefore, both EB1n-EB1n and EB1n-EB1c interactions were relatively weak.

Because only line broadening of peaks was observed, the EB1n-EB1n dimer interface structure could not be generated using a docking method. A previous study reported that K113 and K122 residues were cross-linked by DSS, suggesting that the residues were close to the dimer

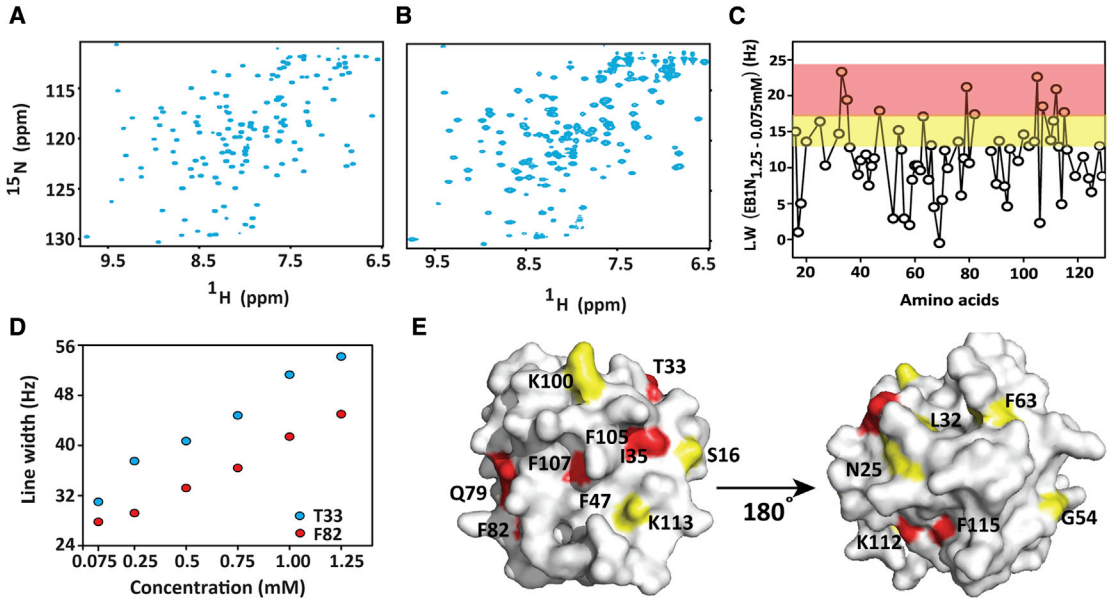

FIGURE 1 The concentration-dependent association of EB1n in solution. (*A* and *B*) ^{1}H-^{15}N HSQC spectra of EB1n at 0.075 and 1.25 mM, respectively. Almost all crosspeaks showed an increase in linewidth at higher concentration. (*C*) The difference in the linewidth of the F2 dimension of crosspeaks of EB1n at 0.075 and 1.25 mM. The region shaded in red was perturbed strongly (above 17 Hz), and the region in yellow showed a medium increase in linewidth (14–17 Hz). (*D*) Change in linewidth of a few representative peaks, T33 (*blue*), and F82 (*red*), with concentration. (*E*) The three-dimensional crystal structure of EB1n (11); the strongly perturbed residues are highlighted in red, and the residues showing medium perturbation are highlighted in yellow. To see this figure in color, go online.

interface (35). We see a significant line broadening for K113 and the surrounding residues, whereas K122 did not show an increase in linewidth. It is likely that the K113 region might be closer to the dimer interface and thereby show line broadening in NMR, whereas K122 could be close enough for DSS cross-linking (<25 Å) but still too distant to show any line broadening effect in NMR.

NMR characterization of full-length EB1

The NMR characterization of individual domains of EB1 (EB1n and EB1c) were known (32,34), but NMR resonance assignments of full-length EB1 residues were not yet determined. The backbone resonances of full-length EB1 were assigned using TROSY-based standard three-dimensional NMR experiments on triple-labeled (^{13}C, ^{15}N, ^{2}H) protein samples. About 80% of the backbone resonances in the TROSY HSQC spectrum of EB1 were identified (BMRB: 50549). However, a number of crosspeaks from EB1c were missing in the TROSY spectrum. The unassigned peaks were mostly from the amino acids located in the linker (loop) region between EB1n and EB1c (Fig. S1; Table S1). Surprisingly, the resonance assignment of most peaks from the individual domains of EB1 matched with those of the full-length protein, suggesting that EB1n-EB1n and EB1n-EB1c interactions were too weak to cause major structure change in the full-length protein. Interestingly, a comparison of the peak position of ^{15}N-^{1}H spectrum of full-length EB1 with EB1n measured at the same experimental conditions showed significant change in the peak positions of two distinct stretches of amino acid (82–89 and 112–115) (Fig. S2, *A* and *B*). In the crystal structure of EB1n (11), these polypeptide stretches, 82–89 and 112–115, were close in space (Fig. S2 *C*). The change in chemical shifts might be due to the interactions present in the full-length protein and absent in EB1n protein. The changes were clearly not due to EB1n-EB1c interactions, as a different set of residues in EB1n were involved in EB1n-EB1c interactions (H18, K62, H69, E70, K100, D125, A128, and R130). Though the second set of residues (112–115) overlapped with the residues involved in EB1n-EB1n interactions, all the residues in EB1n-EB1n dimer interface were not affected in the full-length protein (35). Also, chemical shift changes were absent in the EB1n titration experiments, and EB1n-EB1n association was characterized by only line broadening. Because the EB1n construct contained only a short linker region (20 amino acids), it is feasible that the longer linker region (60 AA) in EB1 full-length protein interacts with the N-terminal domain of EB1, causing the chemical shift changes.

Mapping the binding site of SxIP peptide on EB1

About 50 different +TIP proteins are known to have SxIP signaling motifs with varying degrees of association with EB1 (25,32). Studies also showed that apart from hydrophobic interactions of IP motif in the SxIP peptide signal, electrostatic interaction between positively charged residues

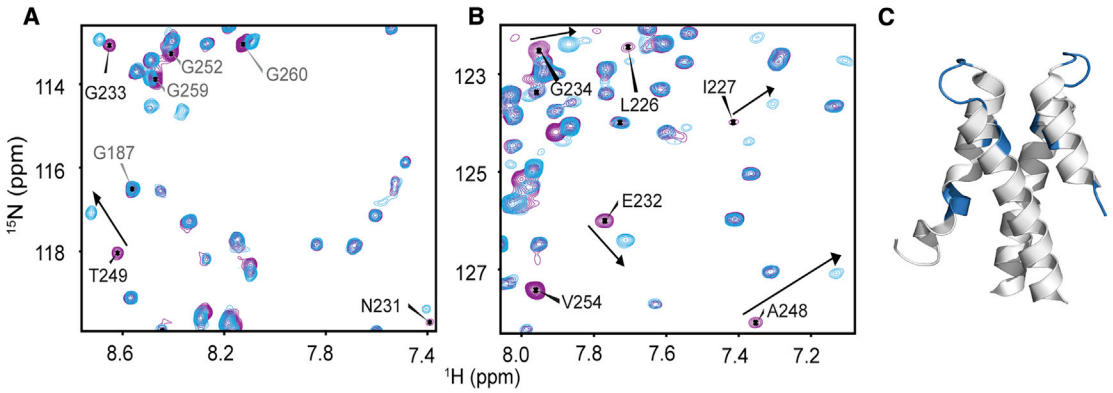

FIGURE 2 (*A* and *B*) Part of the overlaid ^{15}N-^{1}H TROSY spectra of 0.1 mM EB1 in the native (*purple*) and SxIP-peptide-bound form (*blue*). Only the crosspeaks of amino acids from the C-terminal region of EB1 showed significant chemical shift changes. (*C*) The most perturbed region of EB1c (*blue*) in the three-dimensional structure of EB1c (PDB: 1YIG) (17) is similar to the previously reported endogenous peptide binding with EB1. To see this figure in color, go online.

surrounding the SxIP motif and negatively charged residues in the EB1c also played a crucial role in the association process (36,37). Therefore, we chose an SxIP peptide (ALNGQSRIPVLKRHTR) (38) that was previously reported to increase EB1 recruitment to MTs (indicating strong association) for the binding studies. The peptide was synthesized using solid-phase peptide synthesizer and characterized using MALDI (Fig. S3). The bound structure of endogenous SxIP peptide from the +TIP MACF2 with EB1c was already known (33). However, the structural characterization of the selected nonendogenous SxIP-EB1 complex is not known. So, we investigated the interaction between the peptide and full-length EB1 using NMR spectroscopy.

We performed NMR-based titration experiments to determine the intermolecular interaction between the SxIP peptide and EB1. The ^{15}N-^{1}H TROSY spectrum of EB1 (0.1 mM EB1 in 50 mM phosphate-buffered saline, 300 mM KCl, and 1 mM dithiothreitol (pH 6.9)) was measured with increasing peptide concentrations on the 700 MHz NMR spectrometer. The peptide binding perturbed the chemical environment of nuclei around the binding site of the protein, which caused a significant change in the position of NMR peaks in the spectrum (39). By comparing the chemical shifts of the native and peptide-bound protein, the amino acids of EB1 affected by the peptide binding event were identified (Fig. 2, *A* and *B*). The large chemical shift deviations (Fig. S4) for the stretch of amino acids (226–250) constituted the binding site of the peptide. The binding site of the peptide is restricted to the EBH domain of EB1c. Amino acid residues with large chemical shift perturbation were mapped on the crystal structure of EB1c to identify the binding pocket of the peptide (Fig. 2 *C*). The binding pocket of the exogenous peptide (Fig. 2 *C*, highlighted in *blue*) matched with the previously reported interacting region of the native peptide in the crystal structure of EB1c (33).

Apart from the chemical shift perturbation, a decrease in the linewidth (10% decrease in the average line width in ^{1}H dimension) and a corresponding increase in the intensity of NMR signals were noticed (Figs. 3 *A* and S5) for the peptide bound state of EB1. The linewidth and intensity of the NMR peaks depend on the relaxation rate of amide resonances, which in turn rely on the molecular tumbling rate, rate of chemical exchange as well as local spin dynamics. Large proteins and protein complexes tumble slowly in solution, causing an increase in the relaxation rate that leads to NMR signal broadening. A relative decrease in the average line width of NMR signals for the peptide-bound EB1 suggested an apparent reduction in the molecular size. We observed an almost twofold (1.9) increase in the average intensity of NMR peaks of EB1n (Fig. 3 *B*) and a 1.25-fold increase in EB1c peaks (Fig. S5). However, the crosspeaks corresponding to a few amino acids in the EB1n domain showed an intensity increase above 2.0. These residues were R17, M20, I35, E36, C45, K62, K66, F75, I77, L78, Q79, A80, G81, F82, V87, K98, F101, Q102, F105, W110, K112, K113, F114, and F115. The increase in the resonance intensity should be the result of either a decrease in chemical exchange broadening or an increase in local dynamics of the spins. By comparing the differentially affected residues with the residues involved in the EB1n-EB1n interface, it is clear that subset of residues was from the dimer interface of EB1n-EB1n (Fig. S6, K113 region). Also, a few of the residues (36E, 62K, and 100K) were common to both EB1n-EB1c and EB1n-EB1n interfaces. Thus, the line narrowing (intensity increase) of peaks from the EB1n domain of peptide-bound EB1 could be due to the disruption of the EB1n-EB1n and EB1n-EB1c interfaces. Interestingly, the structural region corresponding to the affected residues in EB1n overlaps with the MT interaction interface of EB1 (α4–α6 in Fig. 3 *C*). Therefore, the marked increase in the intensities of the specific residues of EB1 upon SxIP binding should influence the microtubule association of EB1.

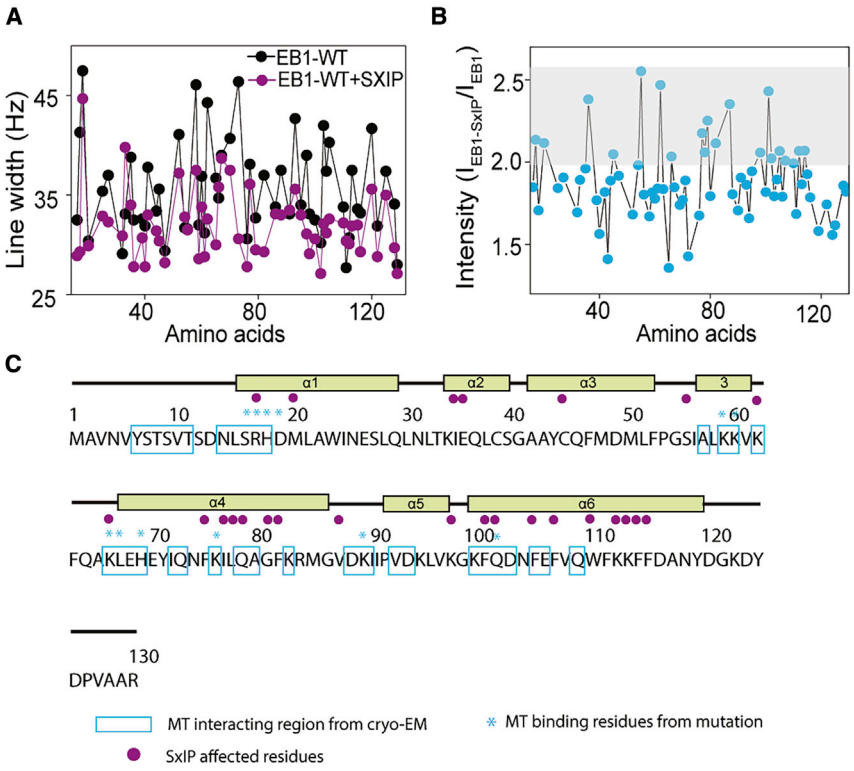

FIGURE 3 (*A*) The N-H linewidths of the residues of N-terminal domain of EB1 from the NMR spectrum of EB1 in the apo form (*black*) and peptide-bound form (*purple*). The average linewidth of peaks decreased with peptide addition. (*B*) The intensity ratio of the NMR peaks from the N-terminal domain of EB1. In the peptide-bound form of EB1, a twofold increase in the intensity of NMR peaks was observed. The shaded region represents amino acids with intensity ratio above 2.0. (*C*) The amino acid sequence of the N-terminal domain (CH domain) of EB1. The amino acids interacting with MTs identified by mutational analysis are in cyan asterisks (13,40). From the cryo-electron microscopy structure of EB1-MT complex, the residues in the CH domain within 5 Å from the tubulin subunit are highlighted by cyan frames (41). The amino acids that are significantly affected by the conformational change induced by the SxIP binding at EB1c are marked as solid purple circles. To see this figure in color, go online.

Peptide-bound EB1 spectrum also revealed 13 new NMR signals that were otherwise absent in the apo EB1 spectrum (Fig. S7). The newly formed NMR peaks belong to the residues located at the structured region of EB1c and close to the EBH domain (Fig. S8). The appearance of new peaks also indicated a possible conformational or dynamical change of EB1 in the SxIP-bound form that decreased the relaxation rate of amide protons and consequently increased the sensitivity of the spectrum.

The SxIP binding promoted the dissociation of native dimer state of EB1

We used diffusion-ordered NMR spectroscopy (DOSY) (42) to determine the effect of peptide binding on the diffusion coefficient of the protein. The diffusion coefficient is used for measuring the size of biomolecules in solution as it reflects the mean-square displacement explored by biomolecules over time (43). DOSY is a pulse-field-gradient-based NMR technique for measuring the diffusion coefficient, in which the displacement of proteins in solution was monitored over time from the variation of intensity of their NMR peaks with increase in applied gradient. Because small molecules diffuse rapidly compared to larger molecules, DOSY experiment should differentiate monomers and dimers in solution. In the DOSY experiment, the gradient was increased from 2 to 95% in 16 steps, and the consequent variation in the intensity of peaks was monitored. The DOSY spectrum of EB1 was measured in the apo form and SxIP-peptide-bound form (100 μM EB1 in phosphate-buffered saline (pH 6.9)). The intensity variation (decay) of aliphatic peaks (less crowded) of the protein centered at 1.2, 1.52, and 2.8 ppm in the DOSY spectrum of EB1 was globally fitted to the well-known Stejskal-Tanner equation (Eq. S1) (Fig. 4 *A*), resulting in a diffusion coefficient of $(5.29 \pm 0.16) \times 10^{-11}$ m^2/s. The DOSY spectrum of SxIP-bound EB1 was measured after incubating the protein with the SxIP peptide. Similar to the apo form, the intensity decay of the NMR peak at 1.2, 1.52, and 2.8 ppm was plotted against the strength of the applied gradients (Fig. 4 *B*). The subsequent global fit of the intensity decay resulted in a diffusion coefficient of $(9.03 \pm 0.2) \times 10^{-11}$ m^2/s. Comparatively, the peptide-bound EB1 diffused rapidly in solution, suggesting a reduction in the size of the protein upon peptide binding.

Assuming a globular protein, the hydrodynamic radius (R_h) of EB1 was calculated from the measured diffusion coefficient using the Stokes-Einstein equation (42). The estimated R_h of EB1 was 5.2 nm. The R_h of EB1 was also calculated using an empirical equation which correlates the protein chain length to the size of the protein (44). The calculated R_h of EB1 in the dimer state was 4.8 nm (2×2.4 nm), in agreement with the experimentally determined value (5.2 nm) from the DOSY spectrum. Hence, the R_h-value from the DOSY spectrum of apo EB1 was similar to EB1 in dimer state in solution (17). The estimated value of R_h from the observed diffusion coefficient of the

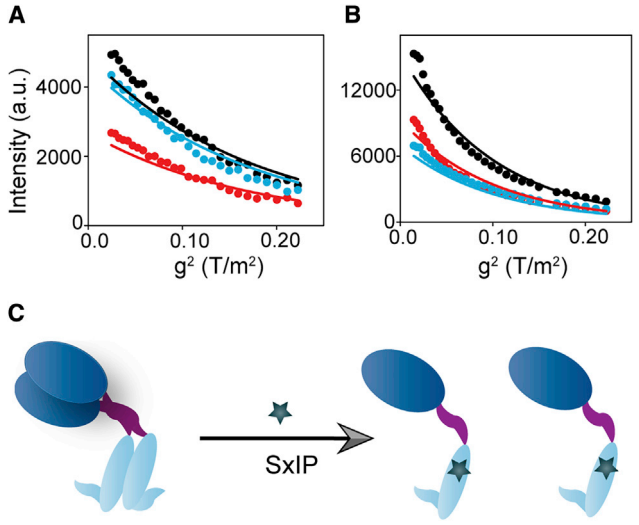

FIGURE 4 (*A* and *B*) The global fit of variation in peak intensities (1.2 ppm (*black*), 1.52 ppm (*blue*), and 2.8 ppm (*red*)) with the applied field gradient. The diffusion coefficients obtained from the global fit were $(5.29 \pm 0.16) \times 10^{-11}$ m^2/s and $(9.03 \pm 0.2) \times 10^{-11}$ m^2/s for EB1 in the apo and the bound forms, respectively. (*C*) Schematic representation of dimer-to-monomer transition of EB1 upon SxIP binding. To see this figure in color, go online.

peptide-bound EB1 was 3.0 nm, similar to the calculated R_h of EB1 in the monomer form (2.4 nm). The R_h derived from the DOSY NMR of EB1 in the apo and peptide-bound state showed that the native EB1 dimer dissociated on binding with the SxIP peptide.

We also compared the rotational correlation time (τ_c) of EB1 in the native and peptide-bound form (Fig. S10; (45)). Under the same experimental conditions, the rotational correlation time of protein increases with protein size. The measured τ_c of apo EB1 was 17 ns. The measured τ_c for the peptide-bound EB1 was 11 ns, which was substantially lower than the protein in the apo form. The dissociation of the dimer to monomeric protein unit upon SxIP peptide binding resulted in the significant decrease in the τ_c-value (Fig. 4 *C*).

SxIP-peptide-induced structural stability of monomeric EB1

Our results consistently showed that the SxIP peptide promoted the dissociation of the native dimeric form of EB1. Hence, the peptide-bound form of full-length EB1 should be stable even in the monomeric state. However, earlier studies suggested that apo EB1 was an obligatory dimer and the native fold of EB1c existed only in the dimeric form (46,47). Thus, we investigated the structural stability of monomeric EB1 in the SxIP-peptide-bound form using an EB1-monomer-specific mutant.

The hydrophobic pocket formed by the residues 222–254 was known to stabilize the native EB1c homodimer. The mutation of a critical residue in the hydrophobic pocket I224 to A224 disrupts the hydrophobic interaction, consequently inducing dissociation of native EB1 homodimer (17,46,48). Through site-directed mutagenesis (49), a plasmid containing the mutant clone (EB1I224A) was generated, and the protein was expressed and purified with established procedure (see Supporting materials and methods; Fig. S11). The ^{15}N-^{1}H TROSY spectrum of EB1I224A was significantly different from wild-type EB1 (Fig. 5). Peaks originating from the EB1c domain of the mutant protein were all clustered around a small spectral window around 8.5 ppm (Fig. 5, *C* and *D*) that is characteristic of unfolded proteins. Apparently, EB1c domain of EB1I224A lost its secondary structure. However, the N-terminal domain of the protein remain folded, and the peaks from the N-terminus of EB1I224A overlayed well with wild-type EB1 spectrum. The I224A mutation collapsed the native fold of EB1c and consequently promoted the dissociation of EB1 from dimer to monomers (Fig. 5 *E*). Thus, EB1I224A should prove to be an excellent model system to understand the structural stability of EB1 monomers induced by the SxIP peptide.

The ^{15}N-^{1}H TROSY spectrum of EB1I224A-SxIP peptide complex was measured at the same experimental conditions as before (Supporting materials and methods). Surprisingly, the crosspeaks of EB1c that originated from its native folded structure started reappearing in the complex (Fig. 6, *A* and *B*). Simultaneously, the peaks (around 8.5 ppm) arising from the unfolded region of the protein reduced in intensity or disappeared (Fig. 6, *C* and *D*).

Moreover, the SxIP-peptide-bound spectra of both EB1I224A and EB1 were found to be similar, suggesting that the SxIP peptide bound to EB1 preserved the conformation of EB1c in the monomer form of EB1 (Fig. 6 *E*). Comparable binding of SxIP peptide on both EB1 (EB1c folded) and EB1I224A (EB1c unfolded) demonstrated that EB1c need not be folded to its native conformation for binding. Even the partially folded state of EB1 can bind SxIP.

The stability of SxIP-bound EB1 monomer was confirmed with molecular dynamics (MD) simulations. We performed two independent 100-ns MD simulations of EB1c monomer (from the crystal structure, PDB: 3GJO (33)), one in the apo form and the other in the SxIP-bound form. The evolution of backbone RMSD (root mean square deviation) of the protein against the simulation time was plotted (Fig. 7 *A*) for the two simulations (bound and unbound). The protein in the apo form showed large deviations from the starting structure (~8 Å). However, RMSD from the starting structure was significantly less (~4 Å) for the simulation of the bound peptide structure. The remarkable stability of the EB1 monomers is clearly demonstrated in the simulation. The decrease in the per-residue RMSF (~2 Å in the amino acid stretch 210–230) of EB1c monomer in the bound form relative to the apo form (Fig. 7 *B*) also implied the conformational stability of SxIP induced EB1c. Additionally, the apo form structure collapsed

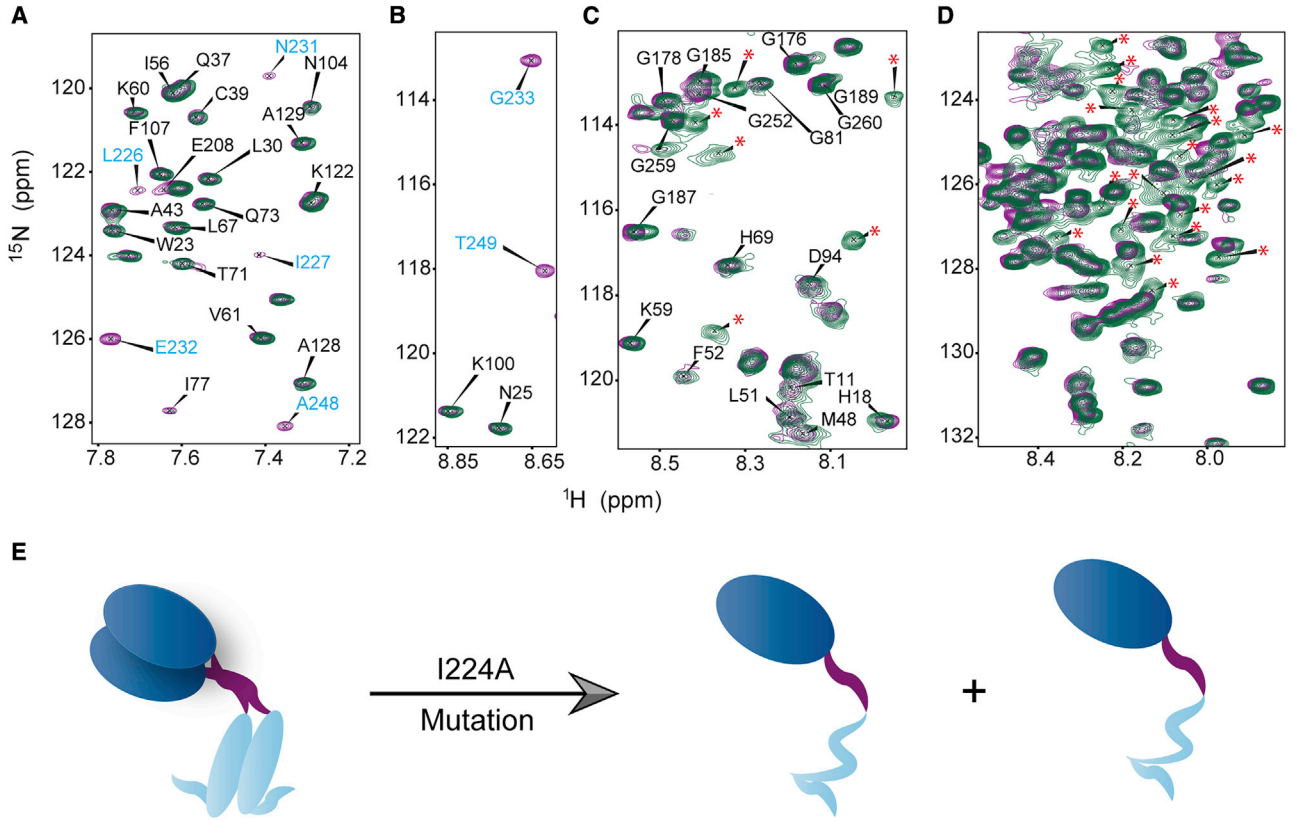

FIGURE 5 (*A–D*) Part of the overlaid ^{15}N-^{1}H TROSY spectra of EB1 (*purple*) and EB1I224A (*green*). The peaks from the structured region of EB1c disappeared (*A* and *B*), and new peaks appeared at 8.5–8.0 ppm (with *asterisk* in *C* and *D*), characteristic of unstructured proteins. The mutation of I224 to A224 resulted in the unfolding of EB1c. (*E*) The schematic representation depicts the structural destabilization of EB1c induced by the I224A mutation. To see this figure in color, go online.

entirely after the MD simulation (C-α RMSD of 6.7 Å relative to the initial structure) (Fig. 7 *C*). In comparison, the peptide-bound form retained the initial structure (C-α RMSD of 3 Å relative to the initial structure) (Fig. 7 *D*). Both experiment and MD simulation suggested that the SxIP peptide maintains the natural folded structure of EB1c and thus stabilizes the monomers of EB1.

Previous studies had shown that EB1n domain was sufficient for the localization of EB1 to the MTs (50). Hence, the dimerization of EB1 promoted by EB1c was not necessary for MT association. The dimerization was supposed to provide structural stability of the native conformation of EB1c. Our results suggested that SxIP peptides preserved the native conformation of EB1c in the monomeric form and promoted the dissociation of EB1 homodimer. We speculate that the dissociation of EB1 might be an essential step in the process of SxIP-mediated MT association of EB1.

SxIP binding reduced the conformational flexibility of the N-terminal domain of EB1

To understand the role of SxIP peptide on the backbone structural dynamics of EB1, we measured ^{15}N-^{1}H heteronuclear NOE (hetNOE) experiment of the protein in both apo and peptide bound forms. Usually, a monotonic decrease in the magnitude of hetNOE values, indicate a gradual increase in the conformational flexibility of the polypeptide backbone in the ps-ns time scale (51). The low hetNOE values (hetNOE value $<$0.6) of residues are a clear indication of a highly flexible protein backbone (51). However, the increase in the magnitude of hetNOE values suggests a decrease in the mobility of the peptide backbone. To directly compare the mobility of apo and peptide-bound forms of EB1, the difference in the hetNOE between the SxIP-bound and apo forms was taken (Figs. 8 and S13). In Fig. 8, ~62% of the peaks were positive, which imply that these amino acids showed an overall increase in the hetNOE values in the bound form compared with the apo form, suggesting an overall decrease in the mobility or conformational flexibility of protein backbone in the bound form. Among the residues in EB1n, H18, T33, and V61 (Fig. 8 *A*) showed a significant increase in the hetNOE values (large positive difference). The amino acid H18 and the amino acid stretch containing V61 were known to bind to the plus end of MTs (34); hence, the reduced flexibility at the MT-binding region of EB1 in the SxIP bound form could also be a factor in increasing microtubule association.

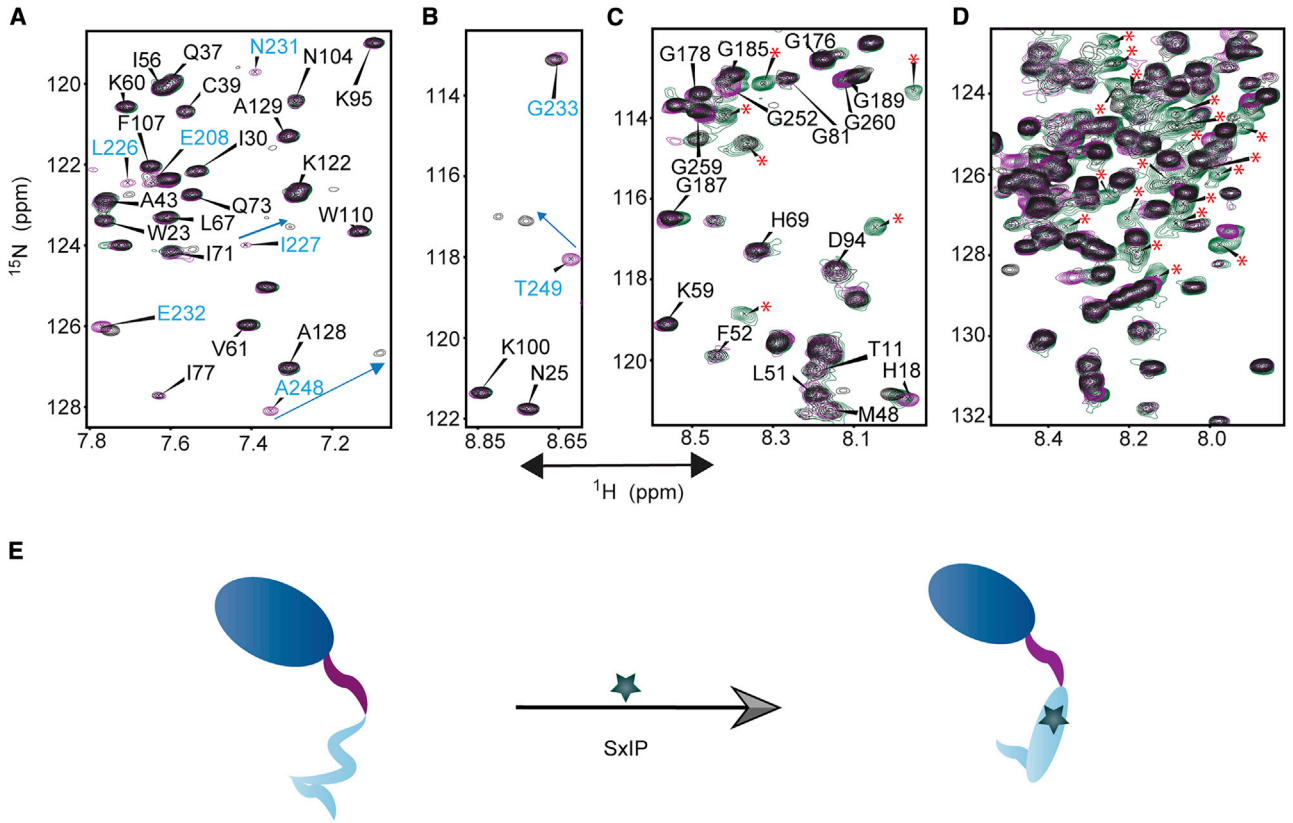

FIGURE 6 (*A–D*) Section of the overlaid ^{15}N-^{1}H TROSY spectra of EB1 (*purple*), EB1I224A (*green*), and EB1I224A + SxIP (*black*). The crosspeaks of EB1c that originated from its native folded structure reappeared in the complex (*blue labeled peaks* in Fig. 7, *A* and *B*). The peaks (labeled by *red asterisk* around 8.5 ppm) arising from the unfolded region of the protein disappeared (Fig. 7, *C* and *D*). The SxIP-bound spectrum of EB1I224A was similar to the peptide-bound spectrum of EB1. (*E*) The schematic representation shows the structural stabilization EB1I224A by SxIP binding. To see this figure in color, go online.

The conformational averaging of EB1 in the apo and the bound form was compared using N-H RDCs (residual dipolar couplings). A 5% Lα phase (52) was used for the RDC measurements such that the deuterium splitting in the two samples was ~21 Hz. The consistent quadrupolar splitting of deuterium (Fig. S12) ensured identical alignment strength for both the apo and SxIP-bound protein samples. Individual N-H RDCs report on the orientation of the amide vector with respect to external magnetic field. In the first approximation, N-H vectors (RDC) report on the structure of the protein. When the amide bonds in a protein have different orientations between the solution and crystal structure, then a fit of the RDCs between the measured and the simulated results (from the crystal structure) will have poor correlation value (R_{corr}). The close agreement between the experimental and simulated RDCs suggest that the structure of the protein in solution is same as that of the crystal structure. The correlation of RDCs of EB1n with and without SxIP fit well with the crystal structure (apo form, $R_{corr} = 0.9$ and $Q = 0.41$; bound form, $R_{corr} = 0.9$ and $Q = 0.4$; Fig. S12), indicating that the structure of the EB1n itself (individual N-H vectors) has not changed from the crystal structure in both the apo form (dimer) and in the peptide-bound form (monomer). This is not surprising because if there were structural changes, a change in chemical shifts would be expected. However, the histograms of ^{1}H-^{15}N RDCs of EB1n in the apo (Fig. 8 *B*) and the SxIP-bound forms (Fig. 8 *C*) of EB1 were different. The distinctive distribution of RDCs in the two histograms indicated that the N-terminal domain of EB1 had different alignment tensors in the absence and presence of SxIP peptide. The alignment tensor reports on the overall shape of the molecule and therefore should be able to distinguish between monomers and dimers. From the distribution of the histogram (Fig. 8 *B*), the magnitude (D_a) and rhombicity (R) of the alignment tensor were determined. A comparative evaluation of D_a-values provides a measure of dynamics of the protein in the liquid crystalline medium (53). The D_a-value estimated from the RDCs in the peptide bound state was larger (8.7 Hz) than the apo EB1 (4.5 Hz). The increase in the D_a-value in the peptide bound EB1 suggested reduced mobility/flexibility of the protein. The rhombicity (R) of the alignment tensor is a measure of the shape and symmetry of the molecule. The magnitude of rhombicity generally ranges from 0 to 0.66, with a perfectly

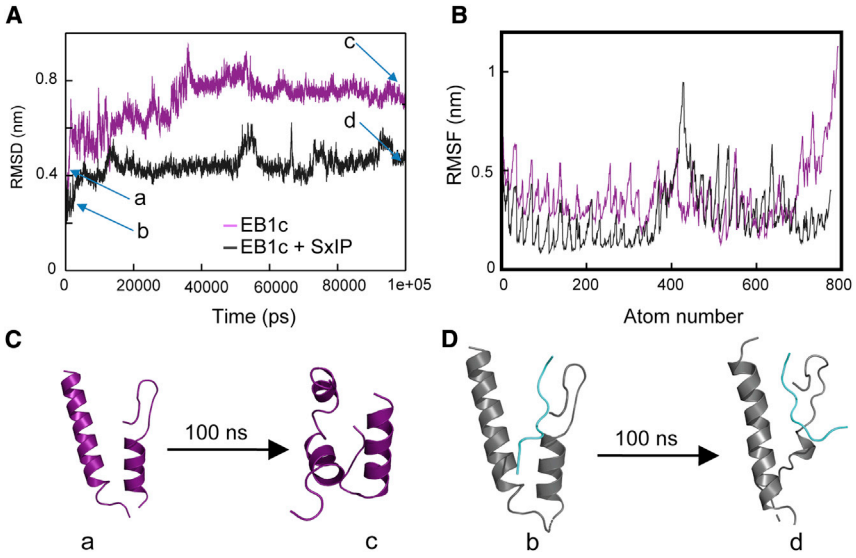

FIGURE 7 (*A*) Variation in the RMSD from the starting structure over 100-ns MD simulation of EB1c monomer in the apo form (*purple*) and bound form (*black*). (*B*) The per-residue RMS fluctuation of EB1 monomer in the apo form (*pink*) and bound form (*black*) during the MD simulation. (*C* and *D*) The cartoon representation of the initial and final structure from the MD simulation of EB1c in the apo form and bound form, respectively. To see this figure in color, go online.

symmetrical (sphere) and an asymmetrical molecule having values 0 and 0.66, respectively. The observed rhombicities in the alignment tensor of EB1n in the apo and bound form of EB1 were 0.598 and 0.354, respectively. The magnitude of rhombicity shows that EB1n has an ellipsoidal alignment tensor (R = 0.598) in the apo form compared with the peptide-bound form (R = 0.354). Hence, from the reduction in rhombicity, we conclude that in the peptide-bound form, EB1n domain is having a symmetric globular shape compared to the apo protein.

In more basic representation, when two spheres are in contact, the combined unit will not be any more spherical. The monomer-dimer shift can thus be monitored by evaluating the alignment tensors from the RDCs. In our case, dimer is the apo form (R = 0.598), which is asymmetrical (cylindrical shape). The peptide-bound forms are the monomers (individual spheres), which are more symmetrical (R = 0.354). Therefore, the decrease in the rhombicity of EB1n on peptide binding also supports the reduced dimer interactions in EB1n domain. The individual amide RDCs of both the apo and bound forms fit well with the crystal structure because the structure of the monomeric unit is same in both the monomeric state and in the dimeric state of the protein.

Previous studies had shown that the dimerization domains of EBs (EB1c) exchange their chains in solution, and the various binding partners of EB1 (CAP-GLY and SxIP) regulate the exchange process (48,50). Our results indicate that SxIP signaling motifs reduce the exchange rate of the EB1c chain by shifting the exchange equilibrium toward the monomeric form of EB1. The broader distribution of RDCs observed in the SxIP bound state of EB1 compared to its apo form was a clear indication of the reduced conformational dynamics of the protein in the bound state. Usually, monomers of a protein are more mobile than the dimer. Surprisingly, the hetNOE values of EB1 (EB1n domain) increased with SxIP binding, suggesting structural rigidity. Hence, it is likely that marked increase in the intensity of peaks observed for some of the residues of EB1n upon SxIP binding (Figs. 3 *A* and S5) could be due to a decrease in chemical exchange broadening, associated with the reduction in the transient EB1n-EB1n and/or EB1n-EB1c interactions. Additionally, the reduced conformational flexibility and the more symmetric alignment tensor of peptide bound EB1n suggested that the transient interactions (EB1n-EB1n and EB1n-EB1c) present in the apo form were reduced in the peptide-bound form. Consequently, in the mechanism of SxIP-induced MT activation of EB1, the dissociation of EB1 homodimers by SxIP could be a crucial intervening step. Hence, in the presence of SxIP signaling motifs, a large fraction of EB1 localizes toward the MTs, presumably in its monomeric form.

In conclusion, the interaction study of EB1 and SxIP peptide in solution revealed that the peptide promoted the dissociation of EB1 from its native dimer form to its monomeric unit. It was already known that dimerization of EB1 was not necessary for the microtubule association (50) and only the N-terminal domain of EB1 was responsible for the binding to microtubule. The dimer formation was thought to provide structural stability of the C-terminal domain, which was otherwise unstable in the monomeric unit. We have shown here that the EB1 monomer was stabilized by the SxIP signal motif. The I224A mutation and subsequent NMR studies revealed that the peptide-bound EB1 was stable even in the monomeric form. The structural stability of the EB1c monomer in the SxIP bound state was also noticed in the MD simulations. Because SxIP binds to EB1 in a 1:1 ratio (48,50), the binding of SxIP to EB1 should be entropically favored with the dissociation of EB1 dimer. We also determined that the binding event at the C-terminus of

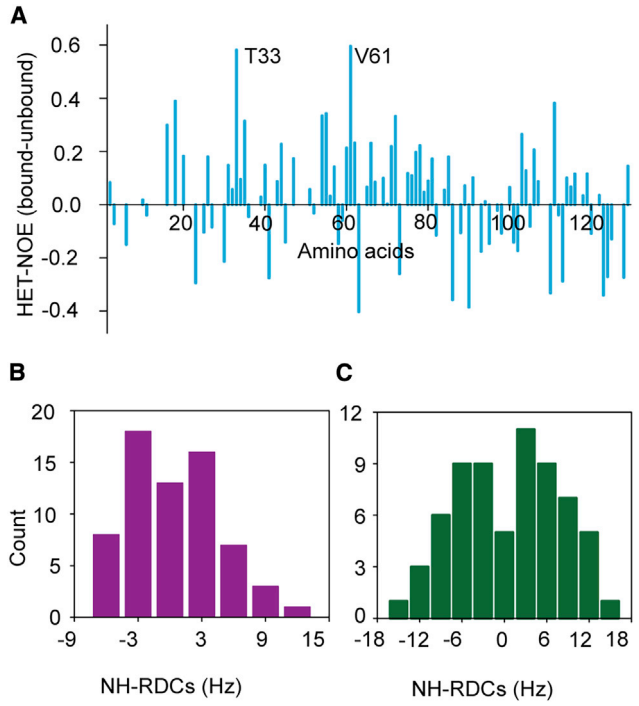

FIGURE 8 (*A*) The difference in the ^{15}N hetNOE of EB1 residues between SxIP-bound and apo forms. The average hetNOE values increased in the peptide-bound state. The amino acids T33 and V61 showed a significant increase in the hetNOE values. (*B* and *C*) The histograms of ^{1}H-^{15}N RDCs for the N-terminal domain of EB1 in the apo and the SxIP-bound EB1, respectively. The different distribution in the two histograms suggests that the N-terminal domain of EB1 has distinct alignment tensors in the absence and presence of SxIP peptide, indicating a change in the overall shape of the protein in the apo and the bound states of EB1. To see this figure in color, go online.

EB1 reduced the dynamics of the EB1 N-terminal domain and specifically the residues in the microtubule-binding site of peptide-bound monomeric EB1. The decline in the dimeric interactions in EB1, coupled with the decreased backbone dynamics of the N-terminal domain, could positively regulate microtubule localization.

SUPPORTING MATERIAL

Supporting material can be found online at https://doi.org/10.1016/j.bpj.2021.03.004.

AUTHOR CONTRIBUTIONS

A.S., T.K.M., and V.V. designed the project. A.S. did the research. A.S. and V.V. analyzed the data and wrote the manuscript. A.K., M.R.R., L.M., and T.K.M. contributed samples.

ACKNOWLEDGMENTS

All authors thank IISER Thiruvananthapuram for funding. V.V. also thanks Science and Engineering Board (SERB) through grant number CRG/2019/004880 for the funding. A.S. thanks CSIR for the fellowship.

REFERENCES

1. Downing, K. H., and E. Nogales. 1998. New insights into microtubule structure and function from the atomic model of tubulin. *Eur. Biophys. J.* 27:431–436.
2. Tilney, L. G., J. Bryan, …, D. H. Snyder. 1973. Microtubules: evidence for 13 protofilaments. *J. Cell Biol.* 59:267–275.
3. Mandelkow, E., and E. M. Mandelkow. 1994. Microtubule structure. *Curr. Opin. Struct. Biol.* 4:171–179.
4. Desai, A., and T. J. Mitchison. 1997. Microtubule polymerization dynamics. *Annu. Rev. Cell Dev. Biol.* 13:83–117.
5. Burbank, K. S., and T. J. Mitchison. 2006. Microtubule dynamic instability. *Curr. Biol.* 16:R516–R517.
6. Mitchison, T., and M. Kirschner. 1984. Dynamic instability of microtubule growth. *Nature.* 312:237–242.
7. Akhmanova, A., and C. C. Hoogenraad. 2005. Microtubule plus-end-tracking proteins: mechanisms and functions. *Curr. Opin. Cell Biol.* 17:47–54.
8. Schuyler, S. C., and D. Pellman. 2001. Microtubule "plus-end-tracking proteins": the end is just the beginning. *Cell.* 105:421–424.
9. Jiang, K., and A. Akhmanova. 2011. Microtubule tip-interacting proteins: a view from both ends. *Curr. Opin. Cell Biol.* 23:94–101.
10. Galjart, N. 2010. Plus-end-tracking proteins and their interactions at microtubule ends. *Curr. Biol.* 20:R528–R537.
11. Hayashi, I., and M. Ikura. 2003. Crystal structure of the amino-terminal microtubule-binding domain of end-binding protein 1 (EB1). *J. Biol. Chem.* 278:36430–36434.
12. Slep, K. C. 2010. Structural and mechanistic insights into microtubule end-binding proteins. *Curr. Opin. Cell Biol.* 22:88–95.
13. Maurer, S. P., F. J. Fourniol, …, T. Surrey. 2012. EBs recognize a nucleotide-dependent structural cap at growing microtubule ends. *Cell.* 149:371–382.
14. Maurer, S. P., P. Bieling, …, T. Surrey. 2011. GTPgammaS microtubules mimic the growing microtubule end structure recognized by end-binding proteins (EBs). *Proc. Natl. Acad. Sci. USA.* 108:3988–3993.
15. Lopez, B. J., and M. T. Valentine. 2016. The +TIP coordinating protein EB1 is highly dynamic and diffusive on microtubules, sensitive to GTP analog, ionic strength, and EB1 concentration. *Cytoskeleton (Hoboken).* 73:23–34.
16. Gireesh, K. K., A. Shine, …, T. K. Manna. 2018. GTP-binding facilitates EB1 recruitment onto microtubules by relieving its auto-inhibition. *Sci. Rep.* 8:9792.
17. Slep, K. C., S. L. Rogers, …, R. D. Vale. 2005. Structural determinants for EB1-mediated recruitment of APC and spectraplakins to the microtubule plus end. *J. Cell Biol.* 168:587–598.
18. Lansbergen, G., and A. Akhmanova. 2006. Microtubule plus end: a hub of cellular activities. *Traffic.* 7:499–507.
19. Xia, P., X. Liu, …, X. Yao. 2014. Superresolution imaging reveals structural features of EB1 in microtubule plus-end tracking. *Mol. Biol. Cell.* 25:4166–4173.
20. Li, W., T. Miki, …, G. Goshima. 2011. EB1 promotes microtubule dynamics by recruiting Sentin in Drosophila cells. *J. Cell Biol.* 193:973–983.
21. Matsuo, Y., S. P. Maurer, …, T. Toda. 2016. An unconventional interaction between Dis1/TOG and Mal3/EB1 in fission yeast promotes the fidelity of chromosome segregation. *J. Cell Sci.* 129:4592–4606.
22. Honnappa, S., O. Okhrimenko, …, M. O. Steinmetz. 2006. Key interaction modes of dynamic +TIP networks. *Mol. Cell.* 23:663–671.
23. Steinmetz, M. O., and A. Akhmanova. 2008. Capturing protein tails by CAP-Gly domains. *Trends Biochem. Sci.* 33:535–545.
24. Kumar, A., C. Manatschal, …, M. O. Steinmetz. 2017. Short linear sequence motif LxxPTPh targets diverse proteins to growing microtubule ends. *Structure.* 25:924–932.e4.

25. Jiang, K., G. Toedt, …, A. Akhmanova. 2012. A Proteome-wide screen for mammalian SxIP motif-containing microtubule plus-end tracking proteins. *Curr. Biol.* 22:1800–1807.

26. Hayashi, I., A. Wilde, …, M. Ikura. 2005. Structural basis for the activation of microtubule assembly by the EB1 and p150Glued complex. *Mol. Cell.* 19:449–460.

27. Weisbrich, A., S. Honnappa, …, M. O. Steinmetz. 2007. Structure-function relationship of CAP-Gly domains. *Nat. Struct. Mol. Biol.* 14:959–967.

28. Serre, L., V. Stoppin-Mellet, and I. Arnal. 2019. Adenomatous polyposis coli as a scaffold for microtubule end-binding proteins. *J. Mol. Biol.* 431:1993–2005.

29. Fong, K. W., F. K. C. Au, …, R. Z. Qi. 2017. Microtubule plus-end tracking of end-binding protein 1 (EB1) is regulated by CDK5 regulatory subunit-associated protein 2. *J. Biol. Chem.* 292:7675–7687.

30. Buey, R. M., I. Sen, …, M. O. Steinmetz. 2012. Sequence determinants of a microtubule tip localization signal (MtLS). *J. Biol. Chem.* 287:28227–28242.

31. Honnappa, S., C. M. John, …, M. O. Steinmetz. 2005. Structural insights into the EB1-APC interaction (vol 24, pg 261, 2005). *EMBO J.* 24:872.

32. Almeida, T. B., A. J. Carnell, …, N. G. Berry. 2017. Targeting SxIP-EB1 interaction: An integrated approach to the discovery of small molecule modulators of dynamic binding sites. *Sci. Rep.* 7:15533.

33. Honnappa, S., S. M. Gouveia, …, M. O. Steinmetz. 2009. An EB1-binding motif acts as a microtubule tip localization signal. *Cell.* 138:366–376.

34. Kanaba, T., R. Maesaki, …, M. Mishima. 2013. Microtubule-binding sites of the CH domain of EB1 and its autoinhibition revealed by NMR. *Biochim. Biophys. Acta.* 1834:499–507.

35. Buey, R. M., R. Mohan, …, M. O. Steinmetz. 2011. Insights into EB1 structure and the role of its C-terminal domain for discriminating microtubule tips from the lattice. *Mol. Biol. Cell.* 22:2912–2923.

36. Kumar, P., and T. Wittmann. 2012. +TIPs: SxIPping along microtubule ends. *Trends Cell Biol.* 22:418–428.

37. Kumar, P., M. S. Chimenti, …, T. Wittmann. 2012. Multisite phosphorylation disrupts arginine-glutamate salt bridge networks required for binding of cytoplasmic linker-associated protein 2 (CLASP2) to end-binding protein 1 (EB1). *J. Biol. Chem.* 287:17050–17064.

38. Leśniewska, K., E. Warbrick, and H. Ohkura. 2014. Peptide aptamers define distinct EB1- and EB3-binding motifs and interfere with microtubule dynamics. *Mol. Biol. Cell.* 25:1025–1036.

39. Williamson, M. P. 2013. Using chemical shift perturbation to characterise ligand binding. *Prog. Nucl. Magn. Reson. Spectrosc.* 73:1–16.

40. Slep, K. C., and R. D. Vale. 2007. Structural basis of microtubule plus end tracking by XMAP215, CLIP-170, and EB1. *Mol. Cell.* 27:976–991.

41. Zhang, R., G. M. Alushin, …, E. Nogales. 2015. Mechanistic origin of microtubule dynamic instability and its modulation by EB proteins. *Cell.* 162:849–859.

42. Pagès, G., V. Gilard, …, M. Malet-Martino. 2017. Pulsed-field gradient nuclear magnetic resonance measurements (PFG NMR) for diffusion ordered spectroscopy (DOSY) mapping. *Analyst (Lond.).* 142:3771–3796.

43. Weljie, A. M., A. P. Yamniuk, …, H. J. Vogel. 2003. Protein conformational changes studied by diffusion NMR spectroscopy: application to helix-loop-helix calcium binding proteins. *Protein Sci.* 12:228–236.

44. Wilkins, D. K., S. B. Grimshaw, …, L. J. Smith. 1999. Hydrodynamic radii of native and denatured proteins measured by pulse field gradient NMR techniques. *Biochemistry.* 38:16424–16431.

45. Lee, D., C. Hilty, …, K. Wüthrich. 2006. Effective rotational correlation times of proteins from NMR relaxation interference. *J. Magn. Reson.* 178:72–76.

46. Sen, I., D. Veprintsev, …, M. O. Steinmetz. 2013. End binding proteins are obligatory dimers. *PLoS One.* 8:e74448.

47. Chen, J., Y. Luo, …, J. Zhou. 2014. Phosphoregulation of the dimerization and functions of end-binding protein 1. *Protein Cell.* 5:795–799.

48. De Groot, C. O., I. Jelesarov, …, M. O. Steinmetz. 2010. Molecular insights into mammalian end-binding protein heterodimerization. *J. Biol. Chem.* 285:5802–5814.

49. Edelheit, O., A. Hanukoglu, and I. Hanukoglu. 2009. Simple and efficient site-directed mutagenesis using two single-primer reactions in parallel to generate mutants for protein structure-function studies. *BMC Biotechnol.* 9:61.

50. Komarova, Y., C. O. De Groot, …, A. Akhmanova. 2009. Mammalian end binding proteins control persistent microtubule growth. *J. Cell Biol.* 184:691–706.

51. Chamberlain, A. K., V. Receveur, …, C. M. Dobson. 2001. Characterization of the structure and dynamics of amyloidogenic variants of human lysozyme by NMR spectroscopy. *Protein Sci.* 10:2525–2530.

52. Ruckert, M., and G. Otting. 2000. Alignment of biological macromolecules in novel nonionic liquid crystalline media for NMR experiments. *J. Am. Chem. Soc.* 122:7793–7797.

53. Jacobs, D. M., K. Saxena, …, K. M. Fiebig. 2003. Peptide binding induces large scale changes in inter-domain mobility in human Pin1. *J. Biol. Chem.* 278:26174–26182.

Biophysical Journal, Volume *120*

Supplemental information

SxIP binding disrupts the constitutive homodimer interface of EB1 and stabilizes EB1 monomer

Shine Ayyappan, Pooja S. Dharan, Arya Krishnan, Renjith R. Marira, Mahil Lambert, Tapas K. Manna, and Vinesh Vijayan

Materials and Methods

Protein Expression in Minimal Media

EB1n, EB1 and EB1I224A were expressed in *E. coli* BL21 (DE3) cells. The bacterial cells were first grown in LB medium until the optical density ($O.D_{600}$) of the culture reached 0.6. Then the cells were spun down and resuspended in minimal media containing $^{15}NH_4Cl$ and ^{13}C-glucose as the source of nitrogen and carbon respectively. For EB1 (30 kDa), and EB1I224A, the per deuteration of the amino acid side chain was necessary, so the minimal media were prepared in D_2O instead of water. Bacterial cells in the minimal media were allowed to grow at 37 ^oC until $O.D._{600}$ increased by 0.1 units. Protein expression was induced by 1 mM IPTG. After five hours of protein expression at 37 ^oC, the pelleted cells were resuspended in lysis buffer (20 mM Tris, 25 mM NaCl, 0.1 mM DTT, 2 mM PMSF and protease inhibitor tablet 1/2, pH - 8), sonicated and then centrifuged at 11000 rpm, 4 ^oC for 1 hour to separate the supernatant from cell debris. For the purification of the proteins, the supernatant protein solutions after sonication were loaded into a Ni-NTA column which was pre-equilibrated with 20 mM Tris buffer containing 50 mM NaCl and 0.1 mM DTT at pH - 8. To eliminate the unbound impurity proteins, the column was washed with 20 mM Tris buffer containing 50 mM NaCl, 0.1 mM DTT and 20 mM imidazole. Finally, the pure proteins were eluted from the column using elution buffer (20 mM Tris, 250 mM NaCl, 0.1 mM DTT and 500 mM imidazole, pH -8). The purity of the eluted protein fractions was checked by SDS-PAGE electrophoresis.

<u>The composition of minimal media</u>

The minimal media was prepared using the recipe given below: For 250 ml of minimal media,

• 225 ml of autoclaved water or D_2O

• 20 ml of M9 salt solution (200 mL of M9 salt solution was prepared by dissolving 12 g Na_2HPO_4, 6 g KH_2PO_4 and 1 g of NaCl in water and finally made upto 200 ml using water).

• 2.5 ml of 0.1 M $MgSO_4$

• 250 µl of 0.5 M $CaCl_2$

• 2.50 ml of 100X MEM Vitamin mixture from GE Healthcare

• 1 g of glucose ($^{12}C_6H_{12}O_6$)

• 250 mg of $^{15}NH_4Cl$

• 2.5 ml of 100X trace solution (100 ml of trace solution is made by dissolving 0.5 g of Sodium salt of EDTA, 0.083 g $FeCl_3.6H_2O$, 0.005 g of $ZnCl_2$, 0.001 g of $CoCl_2.6H_2O$, 0.001 g of $CuCl_2$, 0.16 g of $MnCl_2.6H_2O$ and 0.001 g of H_3BO_3 in water. The pH of the solution was adjusted to 7.0 after adding each compound)

Preparation of anisotropic liquid crystal medium

We made a 16 % stock solution of liquid crystal phase by mixing 50 µl of pentaethylene glycol monododecyl ether (Sigma Aldrich) with 200 µl phosphate buffer (200 mM NaCl) and 50 µl D_2O in a micro centrifuge tube [14]. Then vortexed the mixture thoroughly. To the mixture, about 20 µl of 1-hexanol (Sigma Aldrich) was added in aliquots of 2 µl . After each addition, the mixture was vortexed vigorously. Finally, the formation of liquid crystalline phase was confirmed by measuring the quadrupolar splitting of deuterium. For measuring RDCs of EB1, the 16 % liquid crystalline medium was diluted to 5 % using concentrated protein solution. Before and after measuring the RDCs, the quadrupolar splitting of deuterium in the sample was measured to ensure the stability of the anisotropic medium.

Synthesis and Purification of SxIP peptide

SxIP peptide ("ALNGQSRIPVLKRHTR") was synthesized using automated PS3TM Peptide Synthesizer, which employs Fmoc-based solid phase peptide chemistry [10]. Fmoc protected amino acids and the reagents for the synthesis were purchased from Sigma Aldrich. The peptide synthesis mainly involves four steps in which the first step is the attachment of the C-terminal amino acid of the peptide to a Rink amide MBHA resin (Nova Biochem). The second step involves the deprotection of the N-alpha position. In the next step, activation and coupling of the second amino acid takes place. HBTU ((2-(1H-benzotriazol-1-yl)-1, 1, 3, 3-tetramethyluronium hexafluorophosphate) (Sigma Aldrich) was used as the coupling agent. This cycle is continued till the end of the peptide sequence. N-terminus of the peptide was acetylated using acetic anhydride and piperidine. After the synthesis, the resin was washed with dichloromethane (DCM) and dried. Finally, the side chains were deprotected and the synthesized peptide was cleaved from the resin under nitrogen atmosphere using the cleavage cocktail with the composition: 88 % trifluoroacetic acid (TFA), 5 % phenol, 5 % water and 2 % triisopropyl silane (TIPS) for 2 hours. The cleaved peptide was precipitated in ice cold ether, dried and lyophilized from glacial acetic acid. Later the peptide was purified using reverse phase high-performance liquid chromatography (HPLC) using C18 column with HPLC instrument (Agilent Technologies). After purification, the peptide was lyophilized from water. The purified peptide was characterized using matrix-assisted laser desorption/ionization mass spectrometry.

NMR Titration Experiments

To determine the interaction interface of EB1 and SxIP or EB1I224A and SxIP, ^{15}N-^{1}H TROSY titration experiments were carried out on 700 MHz NMR spectrometer. ^{15}N-^{1}H TROSY of 0.1 mM EB1 or 0.1 mM EB1I224A were measured at increasing SxIP concentrations starting from 0.5 mM to 1.5 mM (0.5 mM, 1 mM, 1.5 mM). For the titration

experiment, 0.1 mM ^{15}N labelled protein was dissolved in 50 mM potassium phosphate buffer consisting of 250 mM KCl, 1 mM DTT, and 10% D_2O at pH 6.9. All the ^{15}N-^{1}H TROSY spectra were acquired with 16 scans and 256 complex points. All the NMR spectra were processed by NMRPIPE and assigned using sparky [11, 12].

Chemical Shift Perturbation (CSP)

For the CSP the chemical shift changes in the ^{15}N and ^{1}H dimensions were combined as follows.

$$\Delta\delta = \sqrt{(\Delta\delta_{HN})^2 + (0.17 * \Delta\delta_N)^2}$$

$\Delta\delta =$ combined chemical shift in Hz

$\Delta\delta_{HN} =$ chemical shift change in the ^{1}H dimension (Hz)

$\Delta\delta_N =$ chemical shift change in the ^{15}N dimension (Hz)

Backbone resonance assignment

The resonances (backbone) of EB1 were assigned using standard 3D NMR experiments such as HNCA, HNCO(CA), HNCO and HNCO(CA). All the 3D experiments were measured on 800 MHz NMR spectrometer. The spectra were processed by NMRPIPE [11] and the sequential assignments were carried out using sparky [12]. Since the resonance assignments of EB1n and EB1c were reported, we compared the resonance assignment obtained in EB1 with the available assignment of its individual domains. The resonance assignment of the individual domains of EB1 matched with those in the full-length protein.

Rotational correlation time (τ_c)

For determining the SxIP peptide induced variation in the τ_C of EB1, TRACT [13] experiments were recorded in the apoform and bound form of EB1. The TRACT experiments use cross-correlated relaxation between chemical shift anisotropy and dipole-dipole relaxation

of amide N-H in the protein [13]. In TRACT, a series of experiments were recorded at different relaxation delay and for each delay two measurements were done, one for the α-spin state, and the other for the β-spin state. The peak integral over the amide region starting from 8.5 ppm to 10 ppm for each spin state was plotted against the relaxation delay. For the relaxation rate, the intensity profile was fitted to a single exponential function.

Diffusion Ordered Spectroscopy (DOSY)

For the DOSY experiment, we used, a 100 μM single labelled (^{15}N) EB1 in 50 mM potassium phosphate buffer (the buffer is prepared in 100 % D_2O to remove the water signal) at pH 6.9. DOSY spectrum was measured with 16 scans and the strength of the gradient was increased from 2 % to 95 % in 16 steps. For processing the data, a non-overlapping aliphatic peak centered at 1.2 ppm, 1.52 ppm and 2.8 ppm were splotted against the applied gradient (Fig. 5 A). The intensity profile was fitted into the equation shown below, for the diffusion coefficient

$$I = I_0 e^{-D\gamma^2 g^2 \delta^2 (\Delta - \delta/3)} \quad \ldots\ldots\ldots (1)$$

I and I_0 denote the intensity of the observed peak with and without the application of gradient pulse. δ is the length of the gradient pulse in millisecond. The gradient strength is g. The gradient strength is increased from 2 % to 98 % in 32 steps. Δ is the delay between two gradient pulses and D is the diffusion coefficient.

MD Simulation

Two independent 100 ns - MD simulations of EB1c monomer were performed, one in the apo form and the other in the SxIP bound form. The initial structure for the MD simulations was extracted from the endogenous SxIP bound crystal structure of EB1c (PDB ID: 3GJO [1]).

The N-terminal stretch of amino acids from E192 to D209 is deleted from the crystal structure of EB1c (3GJO). The apo form of EB1c was obtained by removing the bound SxIP peptide from the crystal structure 3GJO. Hence the starting conformation in the simulation of EB1 apo form and bound form are EB1c (3GJO) from D209 to P256 and EB1c (3GJO) from D209 to P256 with SxIP (K5475-Q5483) respectively. To minimize unwanted motion, acetyl and N-methyl groups were added to the N-terminus and C-terminus respectively. The MD simulations were carried out using GROMACS 5.1.2 package [2-4]. The force field and the solvent model used were AMBER99SB-ILDN and TIP3P respectively [5, 6]. The protein is placed in a cubic box and the distance between the walls of the box and the protein was fixed to 10 Å. In order to neutralize the net charge 0.1 mM Na^+ and Cl^- ions were added to the simulation box containing water and protein. Energy minimization of the solvated systems were done using the steepest descent method [7]. The bonds were constrained using LINCS algorithm [8]. The non-bonded interactions were treated using Particle-mesh Ewald algorithm with a cut off of 10 Å [9]. Each system was allowed to equilibrate in NVT and NPT ensembles for 1 ns. Berendsen thermostat (T=310 K with τ_T = 1 ps) and Parrinello-Rahman barostat (Pressure = 1 bar with τ_P = 1 ps) were used to control the temperature and pressure of the system. The well-equilibrated simulation systems were subjected to 100 ns MD. Trajectories were recorded every 10 ps for further analysis.

Supporting Figures

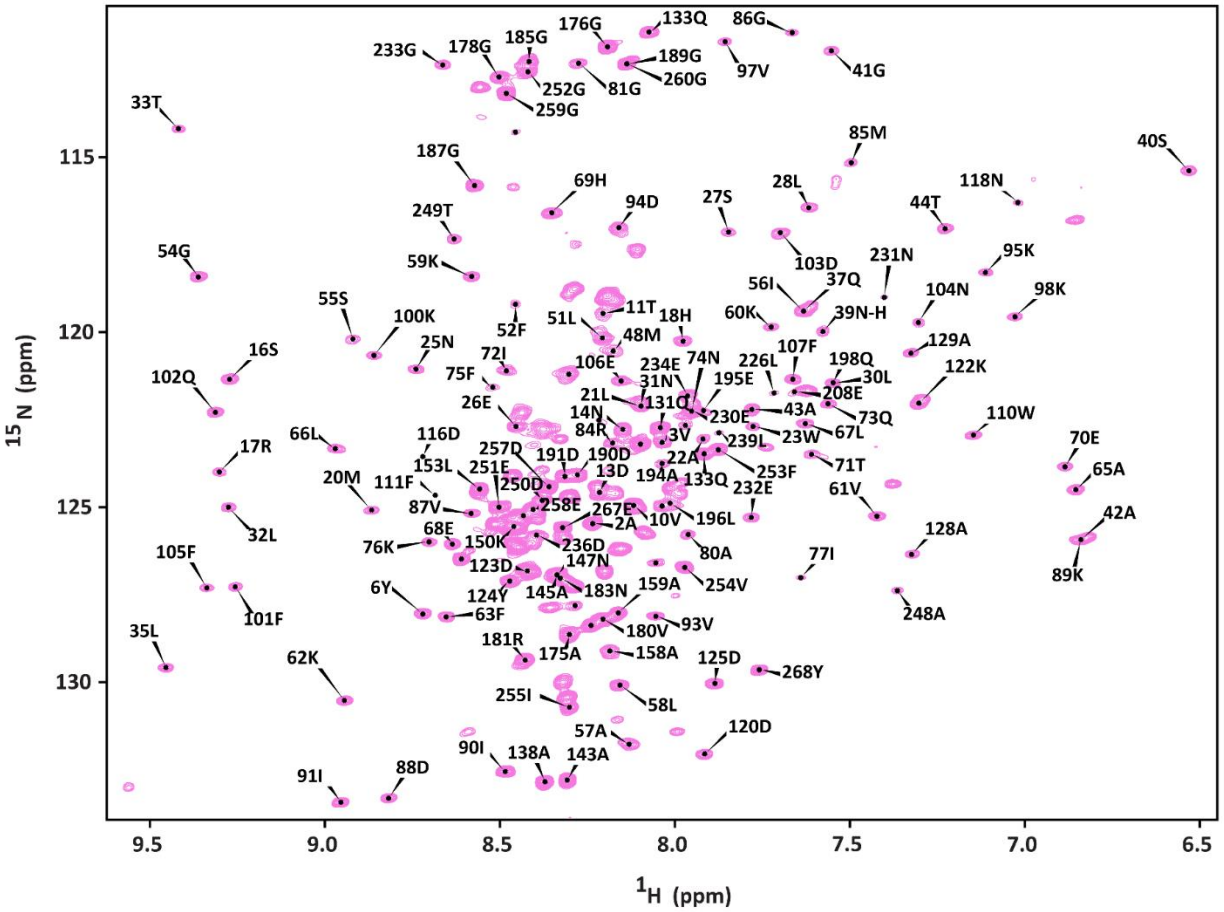

Figure S1. ^{15}N-^{1}H TROSY spectrum of EB1. About 80 % backbone N-H resonances from EB1 were assigned. Incidentally, for most NMR peaks, the resonance assignment of the individual domains of EB1 matched with those in the full-length protein.

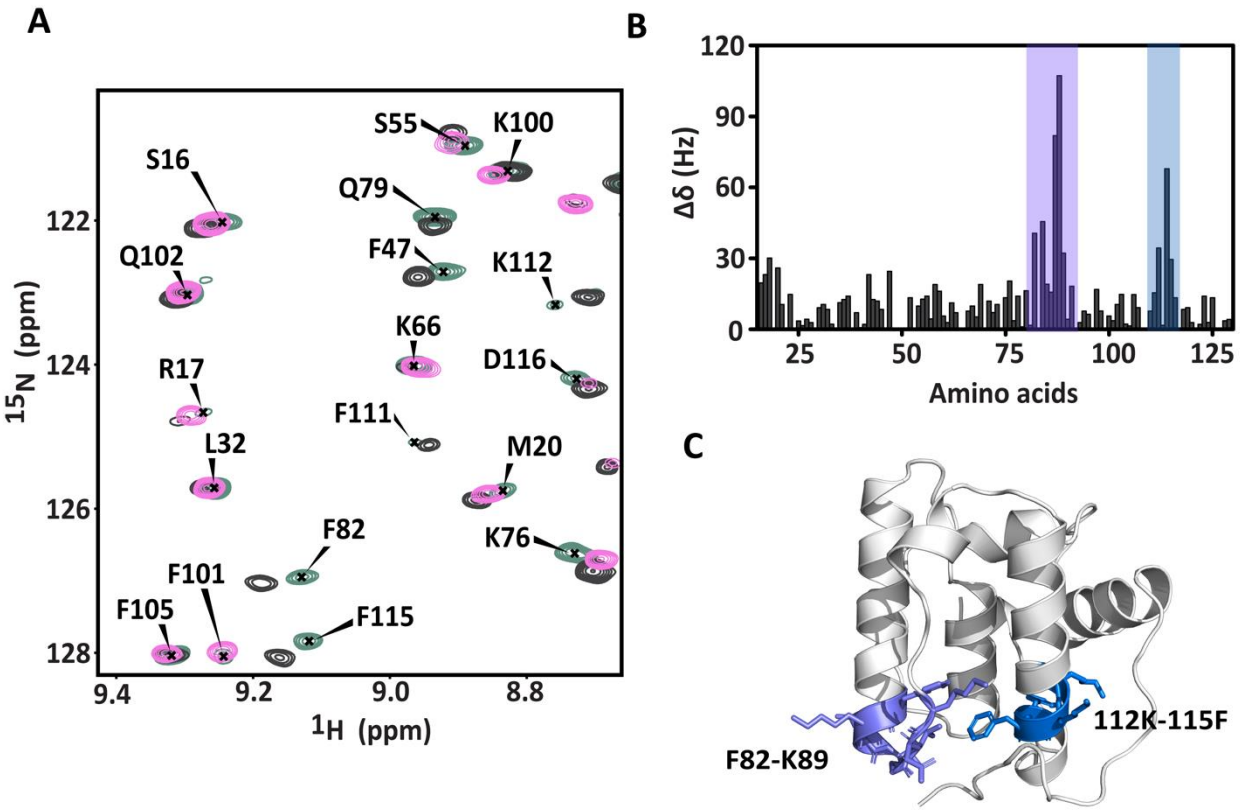

Figure S2. (A) A part of the overlaid ^{15}N-^{1}H TROSY spectra of EB1n (green), non-deuterated EB1 (black) and deuterated EB1 (pink). (B) The quantified chemical shift changes of cross peaks in the spectrum of non-deuterated EB1 relative to EB1n. (C) The two amino acid stretches in non-deuterated EB1 (82-89 and 112-115) that show large chemical shift deviations relative to truncated EB1n is highlighted in the three-dimensional structure of EB1n (1PA7)

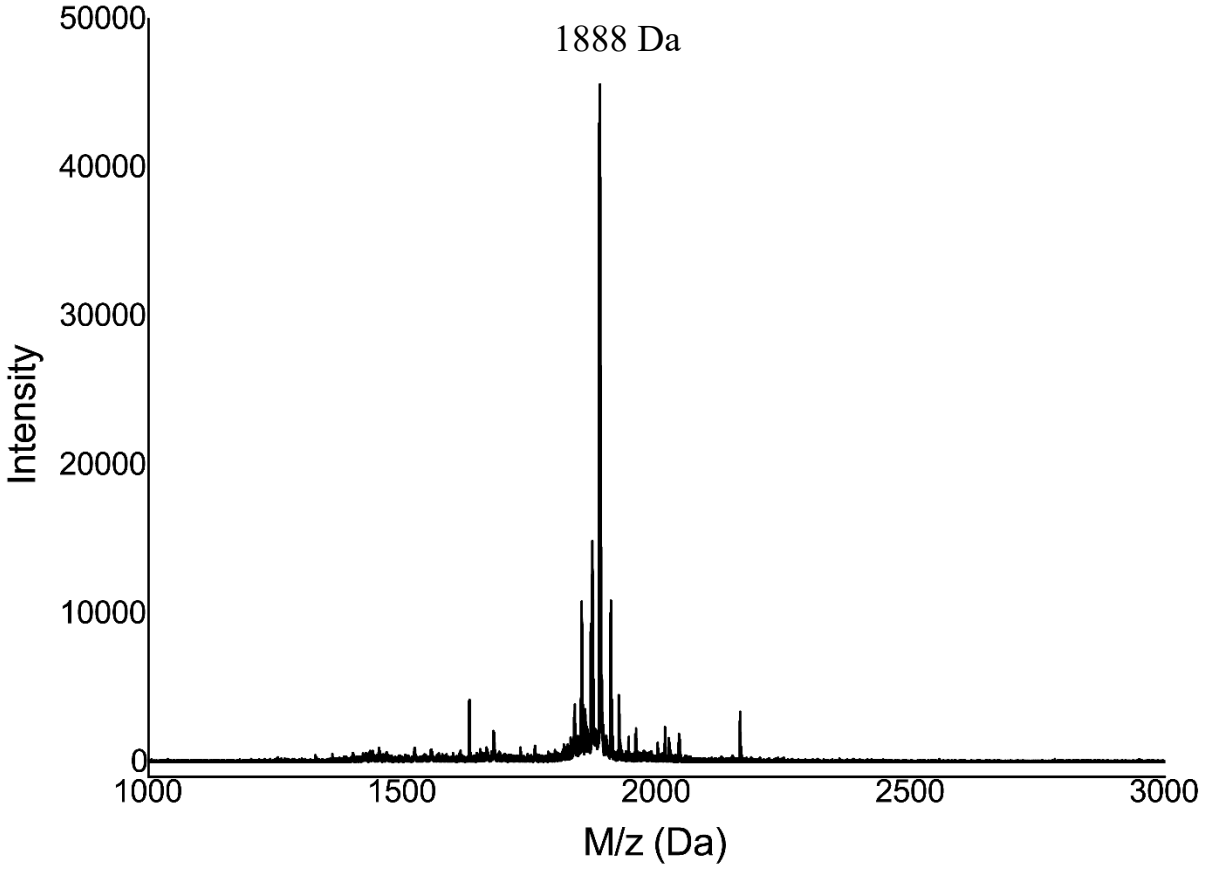

Figure S3. MALDI graph of SxIP peptide aptamer. A high intense molecular ion peak in the graph corresponds to the molecular weight of the peptide.

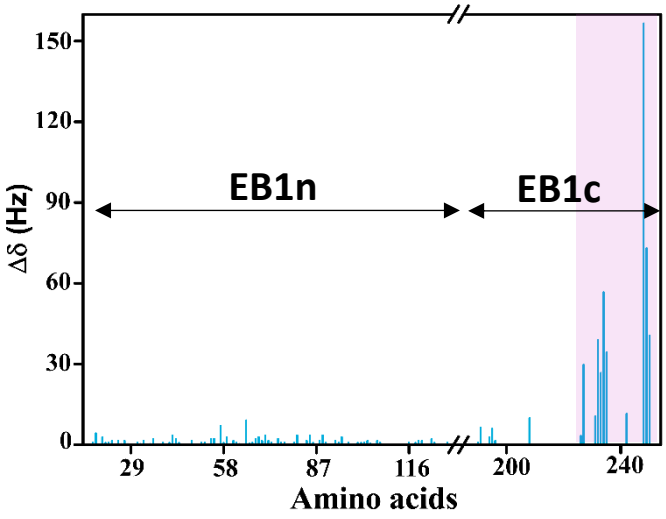

Figure S4. Chemical shift changes of cross peaks in the ^{15}N-^{1}H TROSY spectrum of EB1 with the addition of SxIP peptide aptamer. The amino acids present at the C-terminal region of the protein (226-250) showed large chemical shift deviations.

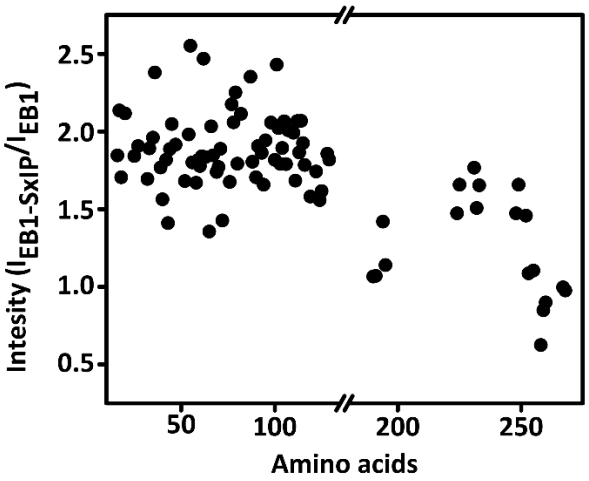

Figure S5. The intensity ratio of the NMR peaks from the N-terminal (1-130) and C-terminal (190-254) domain of EB1. The average intensity ratio of cross peaks from N-terminal and C-terminal domain of EB1 are 1.9 and 1.25 respectively.

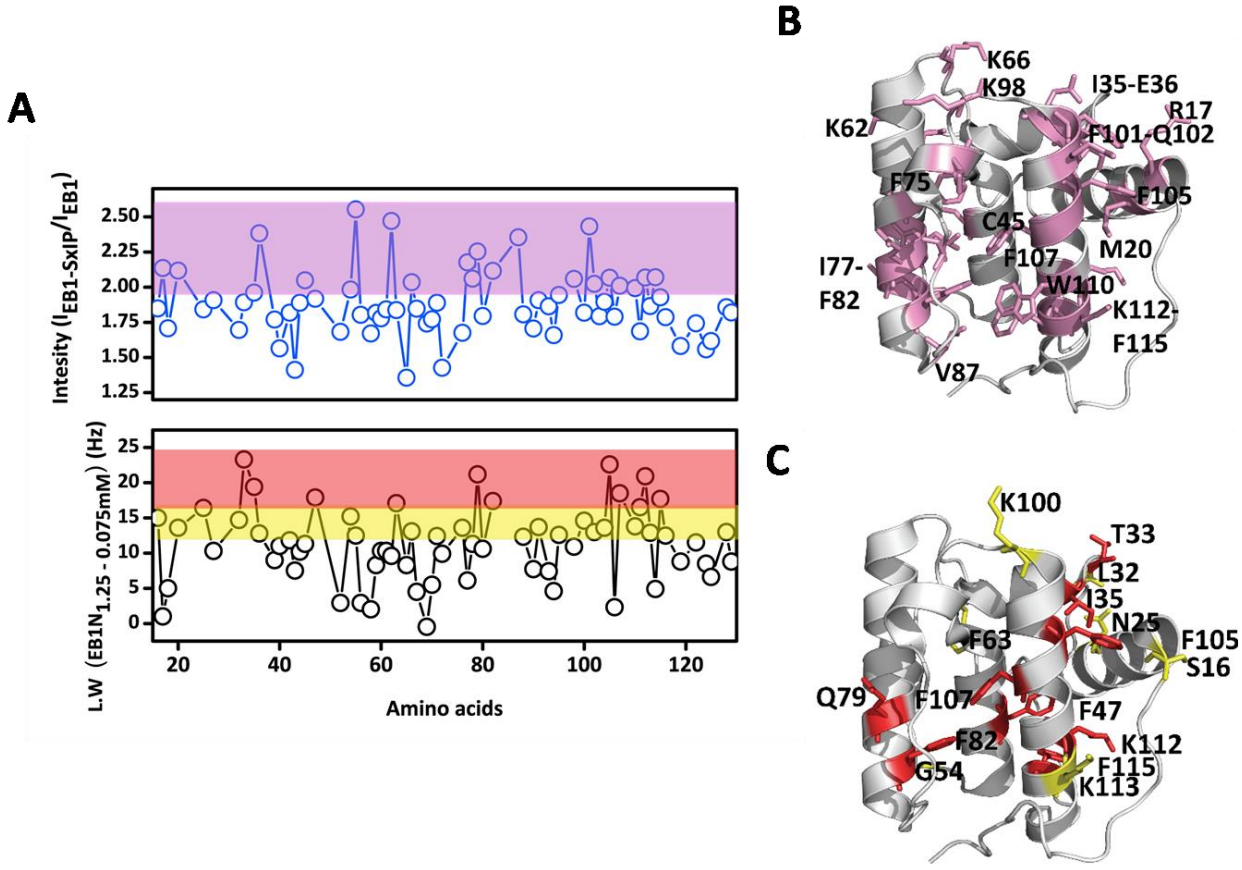

Figure S6. Comparative effect of EB1n-EB1n and EB1-SxIP interaction. (A) The difference in the line width of EB1n residues at 0.075 mM and 1.25 mM and the intensity ratio of residues from EB1n in the SxIP bound form of EB1. (B) Three-dimensional structure of EB1n ("PDB:1PA7") in which the residues showing a significant increase in intensity in the peptide bound form are highlighted. (C) Three-dimensional structure of EB1n ("PDB:1PA7") in which the residues showing large increase in line width during EB1n-EB1n association are highlighted.

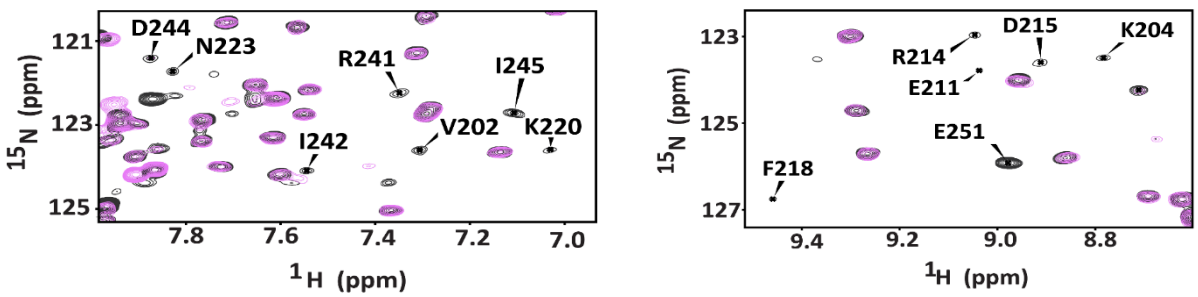

Figure S7. The selected portion in the overlaid ^{15}N-^{1}H TROSY spectrum of the apo form (pink) and SxIP bound form (black) of EB1. The newly appeared peaks in the spectrum of SxIP bound form is labelled, which is absent in the apo form of EB1.

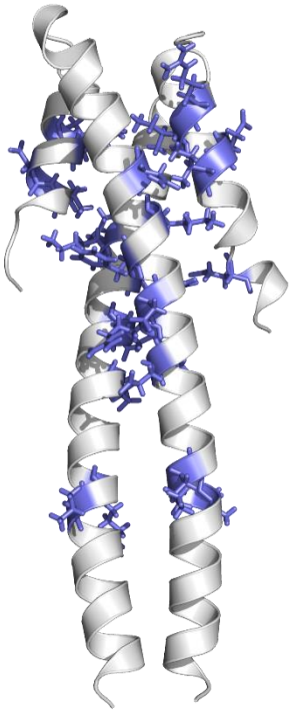

Figure S8. The three-dimensional crystal structure of EB1c ("PDB:1YIG"): the newly appeared NMR peaks with the addition of SxIP peptide are shown in blue. These residues belong to the structured region of EB1c, close to EBH domain.

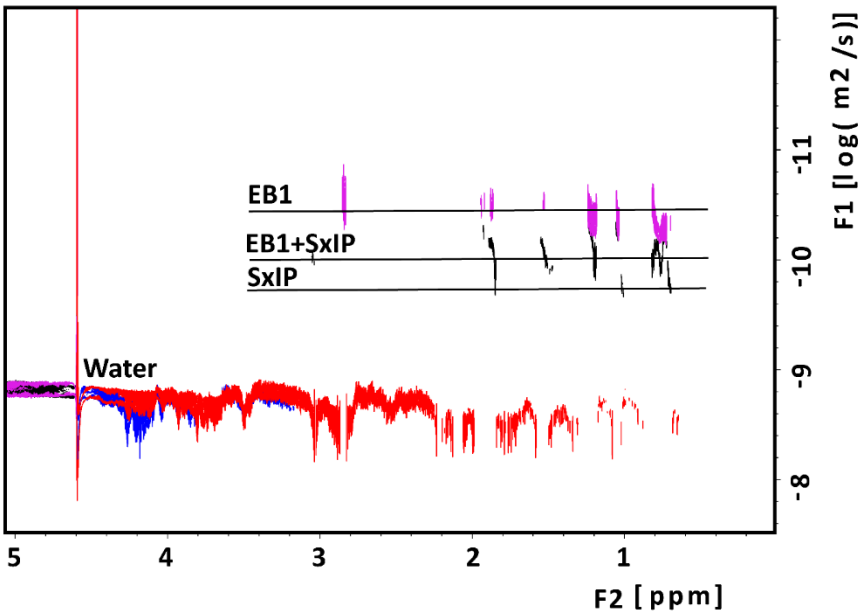

Figure S9. Overlaid DOSY spectrum of EB1 apo form (pink) and EB1-SxIP bound form (black).

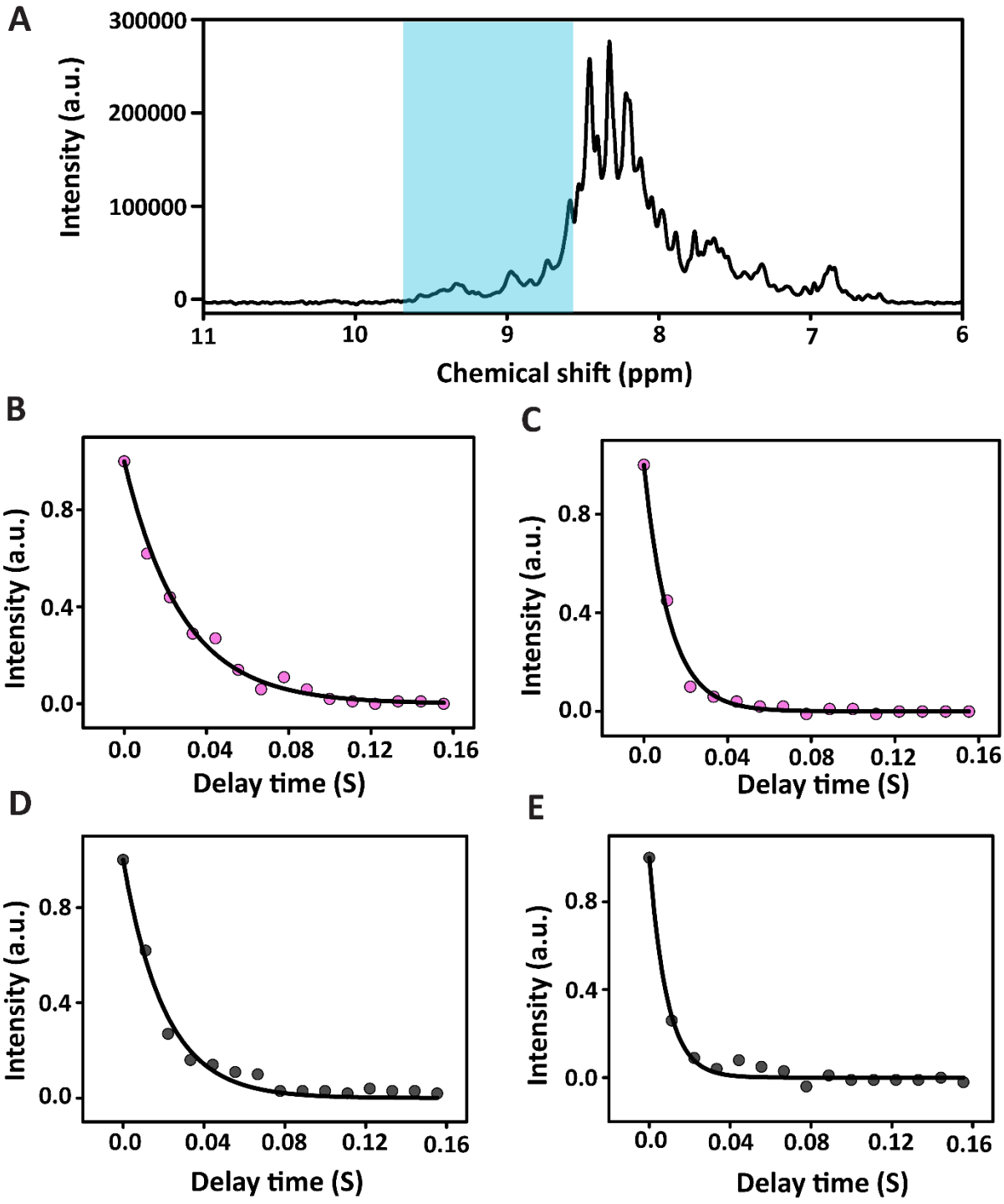
A
300000
200000
100000
0
Intensity (a.u.)
11
10
9
8
7
6
Chemical shift (ppm)
B
0.8
0.4
0.0
Intensity (a.u.)
0.0
0.04
0.08
0.12
0.16
Delay time (S)
C
0.8
0.4
0.0
Intensity (a.u.)
0.0
0.04
0.08
0.12
0.16
Delay time (S)
D
0.8
0.4
0.0
Intensity (a.u.)
0.0
0.04
0.08
0.12
0.16
Delay time (S)
E
0.8
0.4
0.0
Intensity (a.u.)
0.0
0.04
0.08
0.12
0.16
Delay time (S)

Figure S10. (A) the amide region of EB1 from the ^{1}H-^{15}N TRACT experiment. The region used for calculating rotational correlation time is shaded in blue. (A), (B) and (C), (D) show the variation in the intensity of the amide region from 8.6 ppm to 9.75 ppm in the alpha and beta spin states of EB1 in the native (pink) and the peptide-bound (black) forms respectively.

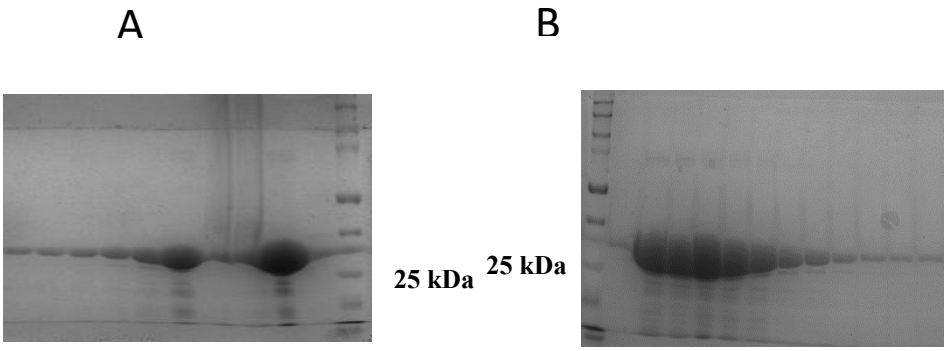

Figure S11. SDS-PAGE image of purified EB1 (A) and EB1I224A (B) protein samples. The thick protein band above 25 kDa corresponds to pure protein.

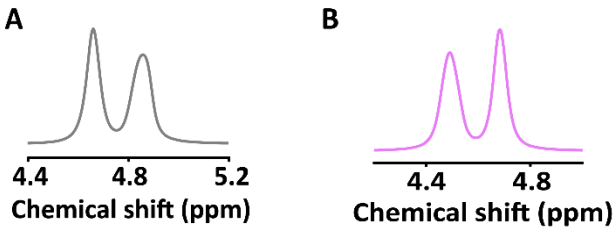

Figure S12. The deuterium quadrupolar splitting observed in the apo form and bound form of EB1. Identical splitting (~ 21 Hz) indicates the similar alignment experienced by the protein in the liquid crystal medium of the two samples.

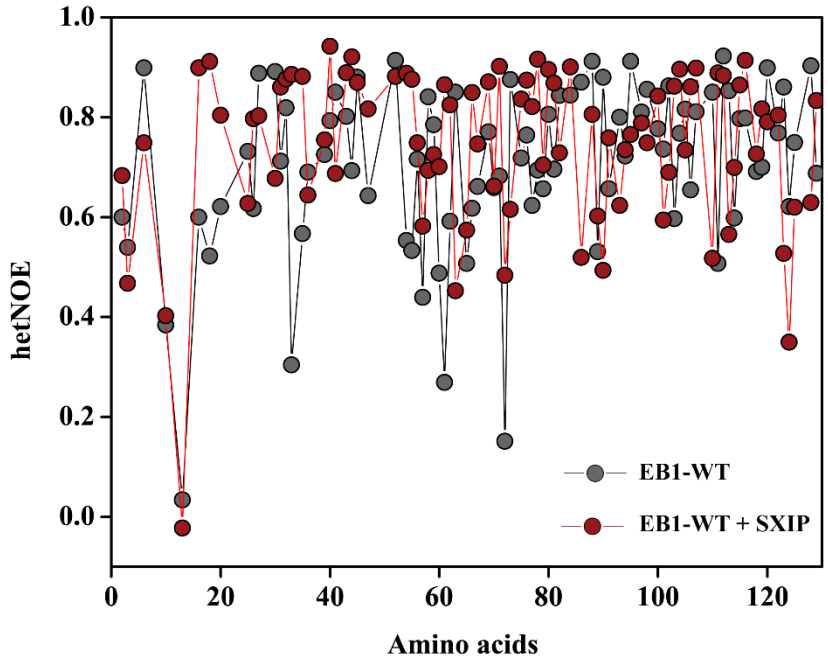

Figure S13. ^{15}N hetNOEs of residues of EB1n domain of EB1 in the apo form (grey) and SxIP bound form (red). The average hetNOE value increased in the peptide-bound form.

Supporting Table

Table S1. Chemical shift assignments of EB1

Residue No.	C_α	CO	H^N	N
S16	57.24	175.3	9.23	121.8
R17	59.96	177.1	9.29	124.8
H18	59.46	178.3	8.02	122.2
M20	57.29	178.2	8.83	125.5
A22	54.86	179.9	7.90	123.6
W23	60.48	178.9	7.77	123.0
E26	58.39	179.1	8.45	122.9
S27	61.92	175.2	7.80	117.5
L28	53.27	176.1	7.60	116.9
Q29	52.22	174.8	7.57	122.0
L30	52.22	175.5	7.59	122.4
N31	51.69	175.2	8.50	112.0
L32	56.45	179	9.25	125.4
T33	60.49	174.9	9.39	114.6
K34	54.75	176.5	7.97	125.1
I35	60.69	177.5	9.42	130.1
E36	61.26	178.3	11.31	123.1
Q37	58.92	178.2	7.58	119.6
C39	58.9	172.3	7.55	120.4
S40	56.35	176.2	6.53	115.8
G41	46.3	173.5	7.54	112.5
A42	55.11	178.5	6.80	126.4
A43	54.63	178.4	7.76	122.6
Y44	60.38	178.3	7.18	117.4

C45	64.19	-	7.46	118.4
M48	-	177	8.15	121.0
L51	-	177.1	8.19	120.5
F52	52.81	-	8.43	119.5
G54	45.16	175.8	9.34	118.9
S55	59.8	174.2	8.82	120.6
I56	57.44	175.1	7.60	119.7
A57	50.27	176.5	8.11	132.1
L58	57.44	178.9	8.14	130.6
K59	57.85	177.4	8.55	118.8
K60	55.46	176.4	7.70	120.3
V61	62.69	175.2	7.40	125.6
K62	53.92	176.3	8.93	131.1
F63	61.91	177.1	8.62	128.6
Q65	52.38	177.2	6.84	125.2
K66	55.71	174.7	8.95	123.8
L67	52.07	176.9	7.60	123.0
E68	60.58	178	8.61	126.5
H69	59.28	178.2	8.34	116.8
E70	57.82	178.4	6.87	124.2
Y71	56.12	179.5	7.61	124.1
I72	66.01	178.3	8.45	121.5
Q73	59.12	179.2	7.56	122.9
N74	55.49	178	8.98	122.7
F75	62.97	178.5	8.50	121.9
K76	59.68	180.5	8.69	126.4
I77	64.97	179.2	7.63	127.3
A80	54.66	181	7.95	126.1

G81	47.6	175.5	8.26	112.6
F82	-	-	9.10	126.9
R84	58.82	177.7	8.17	123.5
M85	52.66	175.9	7.48	115.7
G86	46.58	175.2	7.65	111.8
V87	61.81	176.5	8.53	125.6
D88	53.06	174.8	8.77	133.6
K89	54.19	174.5	6.83	126.7
I90	59.44	176.2	8.46	133.0
I91	59.41	175.8	8.92	134.0
V93	67.58	175.3	8.01	128.5
D94	56.25	177.7	8.14	117.6
K95	57.34	179.5	7.08	118.7
V97	63.69	175.7	7.84	112.2
K98	55.65	178.9	7.00	120.4
G99	46.2	173.7	7.97	132.8
K100	54.43	178.9	8.81	121.0
F101	63.92	177.2	9.23	127.7
Q102	60.17	178.5	9.26	122.6
D103	56.51	179.2	7.67	117.9
N104	56.78	177.7	7.27	120.0
F105	58.34	176.8	9.32	127.7
E106	60.69	179.8	8.14	121.9
F107	61.3	177.2	7.65	113.7
W110	62.09	176.5	7.13	123.4
F111	-	175.9	8.78	124.9
D116	56.69	177.4	8.71	124.2
N118	54.16	174.4	6.98	116.8

Y119	57.52	175.4	8.04	127.3
D120	52.3	176.2	7.90	132.5
K122	56.11	176.5	7.28	122.4
D123	55.72	175.9	8.47	127.0
Y124	57.78	173.3	8.43	127.5
D125	48.7	174.8	7.85	130.3
A128	53.7	180.7	7.30	126.7
A129	-	177.7	7.29	121.2
Q131	55.38	176	8.01	123.0
G132	45.37	174.4	8.05	112.0
Q133	57.27	175.1	7.94	118.7
V137	49.77	175.6	8.33	133.3
V142	118.6	-	7.98	124.4
A143	49.77	175.4	8.27	133.1
A145	51.71	177.7	8.28	127.4
K150	56.05	177	8.42	125.8
L153	55.25	176.1	8.52	124.8
A158	54.85	177	8.15	129.5
A172	49.8	175.5	8.13	128.7
A175	51.59	177.6	8.26	129.0
G176	44.16	171.9	8.15	112.2
G178	45.71	177.8	8.47	113.0
V180	62.08	175.9	8.20	128.5
R181	55.23	175.9	8.39	129.7
N183	53.58	174.5	8.25	127.5
G185	44.98	175.8	8.38	112.6
G187	44.99	174.1	8.54	116.2
N188	53.01	174.4	8.07	112.9

G189	45.43	174.3	8.08	112.4
D190	54.3	176.4	8.25	124.4
D191	54.34	176	8.29	124.5
A194	54.73	179	8.00	124.2
E195	58.56	179	7.92	122.3
L196	59.15	178.5	8.00	125.2
M197	59.05	178	8.31	123.3
K204	60.52	-	8.77	122.8
E208	60.92	180.6	7.60	122.5
E211	60.21	-	8.90	123.3
F218	60.35	176.9	9.39	126.1
G219	44.97	176.5	8.40	114.6
K220	60.07		7.18	123.6
E225	60.58	178.5	8.58	126.8
L226	57.87	-	7.68	122.0
E230	57.27	181.1	7.90	122.7
N231	-	-	7.38	119.3
E232	57.89	177.6	7.76	125.6
G233	45.55	174.5	8.63	112.8
E234	56.04	176.8	7.93	122.4
N235	56.11	174.6	8.28	121.6
D236	51.77	175.3	8.36	126.1
V243	61.1	176.6	8.26	125.0
A248	52.84	179	7.34	127.7
T249	60.42	174.5	8.57	117.6
D250	53.88	175.6	8.33	125.0
E251	56.6	176.7	8.48	125.2
G252	45.05	174.1	8.36	112.7

F253	56.98	174	7.88	123.5
V254	61.83	175	7.89	127.3
I255	58.24	174.7	8.26	131.1
D257	53.88	176.4	8.32	124.6
E258	56.35	177	8.35	125.5
G259	44.96	174.5	8.45	112.8
G260	44.17	171.9	8.10	112.8
E267	55.9	175.1	8.28	125.9
Y268	58.87	-	7.72	130.0

References

[1] Honnappa S, Gouveia SM, Weisbrich A, Damberger FF, Bhavesh NS, Jawhari H, et al. An EB1-Binding Motif Acts as a Microtubule Tip Localization Signal. Cell. 2009;138:366-76.

[2] Berendsen HJC, Vanderspoel D, Vandrunen R. Gromacs - a Message-Passing Parallel Molecular-Dynamics Implementation. Comput Phys Commun. 1995;91:43-56.

[3] Lindahl E, Hess B, van der Spoel D. GROMACS 3.0: a package for molecular simulation and trajectory analysis. J Mol Model. 2001;7:306-17.

[4] Pronk S, Pall S, Schulz R, Larsson P, Bjelkmar P, Apostolov R, et al. GROMACS 4.5: a high-throughput and highly parallel open source molecular simulation toolkit. Bioinformatics. 2013;29:845-54.

[5] Jambeck JPM, Lyubartsev AP. An Extension and Further Validation of an All-Atomistic Force Field for Biological Membranes. J Chem Theory Comput. 2012;8:2938-48.

[6] Mark P, Nilsson L. Structure and dynamics of the TIP3P, SPC, and SPC/E water models at 298 K. J Phys Chem B. 2001;105:24a-a.

[7] Ponder JW, Richards FM. An Efficient Newton-Like Method for Molecular Mechanics Energy Minimization of Large Molecules. J Comput Chem. 1987;8:1016-24.

[8] Hess B, Bekker H, Berendsen HJC, Fraaije JGEM. LINCS: A linear constraint solver for molecular simulations. J Comput Chem. 1997;18:1463-72.

[9] Darden T, York D, Pedersen L. Particle Mesh Ewald - an N.Log(N) Method for Ewald Sums in Large Systems. J Chem Phys. 1993;98:10089-92.

[10] Goux WJ, Kopplin L, Nguyen AD, Leak K, Rutkofsky M, Shanmuganandam VD, et al. The formation of straight and twisted filaments from short tau peptides. J Biol Chem. 2004;279:26868-75.

[11] Delaglio F, Grzesiek S, Vuister GW, Zhu G, Pfeifer J, Bax A. Nmrpipe - a Multidimensional Spectral Processing System Based on Unix Pipes. J Biomol Nmr. 1995;6:277-93.

[12] Goddard TD, Kneller DG. SPARKY 3. University of California, San Francisco, CA. 2008.

[13] Lee D, Hilty C, Wider G, Wuthrich K. Effective rotational correlation times of proteins from NMR relaxation interference. J Magn Reson. 2006;178:72-6.

[14] Ruckert, M., and G. Otting. 2000. Alignment of biological macromolecules in novel nonionic liquid crystalline media for NMR experiments. Journal of the American Chemical Society 122(32):7793-7797.